STRUCTURAL CHEMISTRY

ISSN 2053-2296

Solvent influence on the crystal structures of new cadmium tri-*tert*-butoxysilanethiolate complexes with 1,4-bis(3-aminopropyl)piperazine: luminescence and antifungal activity

Daria Kowalkowska-Zedler,[a] Piotr Bruździak,[b] Zbigniew Hnatejko,[c] Renata Łyszczek,[d] Anna Brillowska-Dąbrowska,[e] Łukasz Ponikiewski,[a] Bartosz Cieśla[a] and Agnieszka Pladzyk[a]*

[a]Department of Inorganic Chemistry, Gdańsk University of Technology, Narutowicza 11/12, Gdańsk 80-233, Poland, [b]Department of Physical Chemistry, Gdańsk University of Technology, Narutowicza 11/12, Gdańsk 80-233, Poland, [c]Department of Rare Earths, Adam Mickiewicz University in Poznań, Uniwersytetu Poznańskiego 8, Poznań 61-614, Poland, [d]Department of General and Coordination Chemistry, Maria Curie-Skłodowska University, PL. M.C. Skłodowska-Curie 2, Lublin 20-031, Poland, and [e]Department of Molecular Biotechnology and Microbiology, Gdańsk University of Technology, Narutowicza 11/12, Gdańsk 80-233, Poland. *Correspondence e-mail: agnieszka.pladzyk@pg.edu.pl

Received 6 April 2023
Accepted 20 June 2023

Edited by L. Dawe, Wilfrid Laurier University, Waterloo, Ontario, Canada

Keywords: antifungal activity; luminescence; solvent influence; crystal structure; hydrogen bonding; thiol; piperazine.

CCDC references: 2192696; 2192695

Supporting information: this article has supporting information at journals.iucr.org/c

Monocrystals of dinuclear μ-1,4-bis(3-aminopropyl)piperazine-$\kappa^4N^1,N^{1'}:N^4,N^{4'}$-bis[bis(tri-*tert*-butoxysilanethiolato-κS)cadmium(II)], $[Cd_2(C_{12}H_{27}O_3SSi)_4(C_{10}H_{24}N_4)]$ or $[Cd_2\{SSi(OtBu)_3\}_4(\mu\text{-BAPP})]$, **1**, and polynuclear *catena*-poly[[bis(tri-*tert*-butoxysilanethiolato-κS)cadmium(II)]-μ-1,4-bis(3-aminopropyl)piperazine-$\kappa^2N^{1'}:N^{4'}$], $[Cd(C_{12}H_{27}O_3SSi)_2(C_{10}H_{24}N_4)]_n$ or $[Cd\{SSi(OtBu)_3\}_2(\mu\text{-BAPP})]_n$, **2**, with 1,4-bis(3-aminopropyl)piperazine (BAPP) and tri-*tert*-butoxysilanethiolate ligands, were obtained from the same ratio of reactants, but with different solvents used for the crystallization processes. The structures and properties of both complexes were characterized using elemental analysis, X-ray diffraction and FT–IR, ^{1}H NMR and luminescence spectroscopy. Applied density functional theory (DFT) computational methods and noncovalent interaction (NCI) analysis were used for geometry optimization and visualization of the interactions between the metallic centres and their surroundings. The X-ray analysis revealed four-coordinate Cd^{II} centres bound to two S atoms of the silanethiolate groups and two N atoms of the BAPP ligand; however, it chelates to tertiary and primary N atoms in **1**, whilst in **2** it does not chelate and bonds only to RNH_2. The photoluminescence properties of complexes **1** and **2** result from free-ligand emission and differ significantly from each other with respect to emission intensity. Additionally, antifungal activity was investigated against 18 isolates of fungi. Compound **1** strongly inhibited the growth of three dermatophytes: *Epidermophyton floccosum*, *Microsporum canis* and *Trichophyton rubrum*.

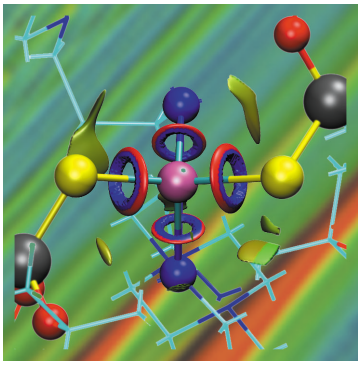

1. Introduction

Piperazine is found to be a structural component of compounds that exhibit interesting properties. Due to its structural similarity to glucose and cyclodextrins, as well as the ability of piperazine N atoms to bind with DNA, this molecule and its derivatives have attracted remarkable interest as ligands in the synthesis of compounds that exhibit anticancer (Nemati *et al.*, 2021; Ragab *et al.*, 2022), antimicrobial (Niemeyer *et al.*, 1979; Keypour *et al.*, 2008) and antimalarial activity (Ryckebusch *et al.*, 2003; Guillon *et al.*, 2017). Piperazine derivatives are also used in the synthesis of metal coordination compounds. One of the promising groups of such complexes are based on cadmium. Despite the toxic properties of the metal itself, the compounds are still studied for the purpose of assessing their

biological activity. However, this is not the only area in which the applicability of cadmium compounds is under investigation, they have also been assessed for their structural, photochemical and catalytic suitability (Wing-Wah Yam *et al.*, 1999; Singh *et al.*, 2015; Keypour *et al.*, 2009; Półrolniczak *et al.*, 2018; Buta *et al.*, 2021).

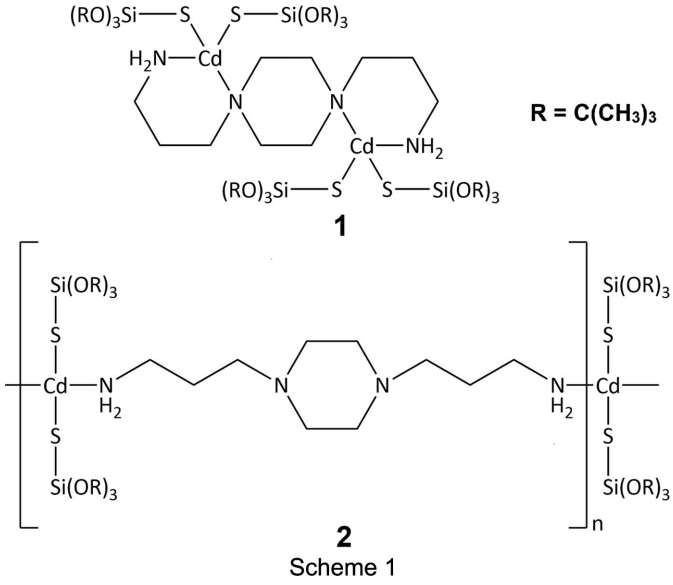

Scheme 1

A detailed analysis of the literature has shown that there are no Cd complexes that contain piperazine derivatives and thiolate residues. This fact is somewhat surprising, as numerous examples show that the presence of thiolate residues in heteroleptic complexes often confers additional physicochemical properties (Henkel *et al.*, 2004; Resta *et al.*, 2010; Gennari *et al.*, 2020; Korkola *et al.*, 2023). Therefore, we have made attempts to synthesize cadmium compounds containing both thiolate and piperazine derivatives as ligands.

Our scientific group is investigating alkoxy- and aryloxysilanethiols, $(RO)_3SiSH$, which are analogues of organic thiols, *R*SH. They contain a C—O—Si—S—H moiety instead of a C—S bond and act as both *S*-terminal and *O*,*S*-chelating ligands in the synthesis of coordination compounds (Pladzyk *et al.*, 2021). The compound commonly used by us in the syntheses of silanethiolates is tri-*tert*-butoxysilanethiol, $(t\mathrm{BuO})_3SiSH$ (TBST). Due to its spatial structure, it shows remarkable resistance towards hydrolysis of the Si—S bonds, allowing for synthesis under atmospheric conditions, giving mono-, di- or polymeric complexes of various metals. Our research focuses on the design and preparation of heteroleptic metal silanethiolates that exhibit luminescence, magnetic and/or catalytic features (Pladzyk *et al.*, 2021). One group of such derivatives is cadmium silanethiolates and our current research is directed towards recognizing the role of 1,4-bis(3-aminopropyl)piperazine (BAPP) in the structural, spectral and cytotoxic properties of cadmium tri-*tert*-butoxysilanethiolates containing this ligand. For this purpose, we conducted reactions using the same molar ratios of cadmium silanethiolate, $[Cd\{SSi(O\mathit{t}Bu)_3\}_2]_2$ (Wojnowski *et al.*, 1992), and BAPP in two different solvent systems. As a result, two new cadmium(II) complexes were obtained, namely, $[Cd_2\{SSi(O\mathit{t}Bu)_3\}_4(\mu\text{-BAPP})]$, **1**, and $[Cd\{SSi(O\mathit{t}Bu)_3\}_2(\mu\text{-BAPP})]_n$, **2**, and their crystal structures, combined with their theoretical studies, spectral characterization and cytotoxic characteristics, are presented below.

2. Experimental

2.1. General procedures

The elemental analyses (C, H, S and N contents) were performed with a Vario EL Cube CHNS apparatus. The FT–IR spectra were measured for crystalline compounds **1** and **2** in the range 4000–400 cm^{-1} with a Nicolet iS50 FT–IR spectrometer equipped with a Specac Quest single-reflection diamond attenuated total reflectance (ATR) accessory. ^{1}H NMR spectra were recorded in solution on a Bruker AV400 MHz spectrometer [external standard: tetramethylsilane (TMS)]. Luminescence spectra in the UV–Vis range were recorded at room temperature on a Hitachi F7000 spectrophotometer equipped with a 150 W xenon lamp as the light source. Thermal analysis of both cadmium complexes in air was performed by thermogravimetric (TG) and differential scanning calorimetry (DSC) methods using a Setsys 16/18 Setaram analyzer. The samples (about 8 mg) were heated in aluminium crucibles in the temperature range 30–1000 °C in flowing air with a heating rate of 10 °C min^{-1}. Thermal analysis under a nitrogen atmosphere was performed using a Q5000 TA apparatus. Samples of about 20 mg were heated to 700 °C at a rate of 20 °C min^{-1} in flowing nitrogen.

2.2. Syntheses

$[Cd\{SSi(O\mathit{t}Bu)_3\}_2]_2$ was obtained according to procedures described previously (Wojnowski *et al.*, 1992). All other reagents were obtained commercially and were used with no further purification.

2.2.1. $[Cd_2\{SSi(O\mathit{t}Bu)_3\}_4(\mu\text{-BAPP})]$, 1. A portion of BAPP (0.082 ml, 0.4 mmol) was added to the solution of $[Cd\{SSi(O\mathit{t}Bu)_3\}_2]_2$ (0.1 mmol, 0.13 g) in methanol (25 ml). The mixture was left at 4 °C for crystallization and after one week colourless crystals of **1** were obtained (yield 60%; m.p. 163.5–164.9 °C). Analysis calculated (%) for $C_{58}H_{132}Cd_2N_4O_{12}S_4Si_4$: C 45.14, H 8.62, N 3.63, S 8.31; found: C 45.14, H 8.57, N 3.65, S 8.35. IR (solid state): ν 3331 (*w*), 3246 (*w*), 3161 (*vw*), 2971 (*vs*), 2930 (*m*), 2903 (*m*), 2858 (*w*), 1584 (*w*), 1471 (*w*), 1418 (*vw*), 1386 (*m*), 1361 (*s*), 1339 (*vw*), 1311 (*vw*), 1285 (*vw*), 1266 (*vw*), 1231 (*m*), 1210 (*m*), 1175 (*s*), 1137 (*w*), 1120 (*w*), 1091 (*vw*), 1083 (*vw*), 1036 (*vs*), 1012 (*s*), 1006 (*vs*), 998 (*vs*), 993 (*vs*), 974 (*m*), 952 (*m*), 912 (*w*), 882 (*vw*), 858 (*vw*), 813 (*m*), 793 (*w*), 734 (*vw*), 723 (*vw*), 688 (*m*), 677 (*m*), 657 (*m*), 607 (*vw*), 535 (*m*), 502 (*w*), 479 (*w*), 470 (*w*), 422 (*w*). ^{1}H NMR (CH_3OH-d_4): δ 4.88 and 3.33 (methanol protons), 2.77 (*t*, 2H, J_{HH} = 6.9 Hz), 2.49 (*t*, 2H, J_{HH} = 7.2 Hz) and 1.73 (*q*, 2H, J_{HH} = 6.8 and 7.1 Hz) – methylene protons of BAPP; 2.62 (*br m*, NH_2 protons of BAPP); 1.42 (*s*, 54H, *t*Bu protons).

2.2.2. $[Cd\{SSi(O\mathit{t}Bu)_3\}_2(\mu\text{-BAPP})]_n$, 2. $[Cd\{SSi(O\mathit{t}Bu)_3\}_2]_2$ (0.1 mmol, 0.13 g) in toluene (8 ml) was mixed with BAPP

Table 1
Experimental details.

For both structures: monoclinic, $P2_1/n$. Experiments were carried out at 120 K with Mo $K\alpha$ radiation using a Stoe IPDS 2T diffractometer. H atoms were treated by a mixture of independent and constrained refinement.

	Monomer **1**	Polymer **2**
Crystal data		
Chemical formula	$[Cd_2(C_{12}H_{27}O_3SSi)_4(C_{10}H_{24}N_4)]$	$[Cd(C_{12}H_{27}O_3SSi)_2(C_{10}H_{24}N_4)]$
M_r	1543.07	871.7
a, b, c (Å)	9.6433 (2), 29.0546 (4), 14.5665 (2)	16.424 (5), 16.876 (4), 18.265 (5)
β (°)	91.466 (1)	112.66 (2)
V (Å^3)	4079.94 (12)	4672 (2)
Z	2	4
μ (mm^{-1})	0.73	0.65
Crystal size (mm)	0.44 × 0.26 × 0.14	0.38 × 0.34 × 0.3
Data collection		
Absorption correction	Multi-scan [*LANA* (Koziskova *et al.*, 2016) in *X-AREA* (Stoe & Cie, 2016)]	Multi-scan [*LANA* (Koziskova *et al.*, 2016) and *X-RED32* in *X-AREA* (Stoe & Cie, 2016)]
T_{min}, T_{max}	0.409, 1.000	0.664, 0.970
No. of measured, independent and observed [$I > 2\sigma(I)$] reflections	39464, 8337, 7133	33547, 9535, 8345
R_{int}	0.028	0.045
$(\sin\theta/\lambda)_{max}$ (Å^{-1})	0.625	0.625
Refinement		
$R[F^2 > 2\sigma(F^2)]$, $wR(F^2)$, S	0.044, 0.123, 1.04	0.043, 0.107, 1.14
No. of reflections	8337	9535
No. of parameters	424	476
$\Delta\rho_{max}$, $\Delta\rho_{min}$ (e Å^{-3})	1.52, −0.71	1.32, −0.74

Computer programs: *WinXpose*, *Recipe*, *Integrate* and *X-RED32* in *X-AREA* (Stoe & Cie, 2016), *SHELXT2014* (Sheldrick, 2015*a*), *SHELXL2018* (Sheldrick, 2015*b*), *ORTEP-3 for Windows* (Farrugia, 2012), *Mercury* (Macrae *et al.*, 2020), *WinGX* (Farrugia, 2012) and *OLEX2* (Dolomanov *et al.*, 2009).

(0.082 ml, 0.4 mmol) dissolved in methanol (2 ml). After gentle stirring, the mixture was allowed to stand for a few days at −20 °C. The obtained white precipitate was filtered off and recrystallized from toluene. Colourless crystals of **2** were obtained after two weeks of crystallization (yield 54%; m.p. 118.4–119.7 °C). Analysis calculated (%) for $C_{34}H_{78}CdN_4O_6S_2Si_2$: C 46.85, H 9.02, N 6.43, S 7.36; found: C 46.71, H 9.14, N 6.44, S 7.12. IR (solid state): ν 3293 (*m*), 3227 (*w*), 3152 (*w*), 2968 (*vs*), 2944 (*m*), 2934 (*m*), 2925 (*m*), 2872 (*w*), 2820 (*m*), 2778 (*w*), 2743 (*vw*), 2723 (*vw*), 2706 (*vw*), 2673 (*vw*), 1590 (*w*), 1492 (*vw*), 1458 (*w*), 1449 (*w*), 1383 (*m*), 1361 (*s*), 1347 (*w*), 1310 (*vw*), 1301 (*w*), 1263 (*w*), 1251 (*w*), 1239 (*m*), 1204 (*m*), 1185 (*s*), 1146 (*w*), 1128 (*w*), 1104 (*w*), 1074 (*w*), 1069 (*w*), 1040 (*vs*), 1004 (*vs*), 987 (*vs*), 961 (*m*), 940 (*w*), 910 (*w*), 882 (*vw*), 842 (*vw*), 820 (*m*), 802 (*m*), 770 (*w*), 728 (*vw*), 683 (*m*), 650 (*s*), 544 (*m*), 500 (*w*), 485 (*w*), 477 (*w*), 461 (*w*), 427 (*vw*), 422 (*w*). ^{1}H NMR (toluene-d_6): δ 2.54 (*br t*, 4H, methylene protons of BAPP), 2.45 (*br m*, 4H, NH_2 protons of BAPP), 2.17 (*t*, J_{HH} = 6.4 Hz, 4H, methylene protons of BAPP), 1.38 (*s*, 54H, *t*Bu protons), 1.26 (*br m*, 4H, methylene protons of BAPP); about 0.9 (very *br m*, 4H of methylene protons of BAPP).

2.3. X-ray crystallography

Crystal data, data collection and structure refinement details are summarized in Table 1. H atoms bonded to C atoms were refined using a riding model. The U_{iso}(H) values of the methyl H atoms were set to 1.5U_{eq}(C), while the U_{iso}(H) values of the H atoms bonded to the remaining C atoms were set to 1.2U_{eq}(C). All H atoms bonded to N atoms were refined freely. The structure of **1** contained a high residual electron-density peak located near atoms S1, S2 and N2. Both S atoms in **1** were refined as positionally disordered over two positions using the PART 1 and PART 2 commands (occupancies 0.79 and 0.21) and the data was calculated with 21.000 and −21.000.

2.4. DFT calculations and NCI analysis

All quantum mechanical calculations were performed with the help of the supercomputers of the Centre of Informatics Tricity Academic Supercomputer & Network Academic Computer Center (TASK, Gdańsk, Poland) with *GAUSSIAN2016* software (Frisch *et al.*, 2016). The structures of the Cd complexes obtained from the diffraction studies were optimized at the M-11L/def2SV(P) level of theory (Peverati *et al.*, 2012; Weigend *et al.*, 2005) with an ultrafine grid and tight convergence criteria. IR frequencies were calculated with the same level of theory and none of these optimized structures exhibited negative frequencies. The selected M-11L functional is optimal for transition metals, organometallic compounds and the determination of noncovalent interactions (NCIs), while the selected basis set provides qualitatively accurate results within a reasonable calculation time. Larger basis sets were tested but turned out to be inefficient for such large molecular complexes (over 200 atoms). Electron densities, a by-product of every density functional theory (DFT) calculation, have been saved to external files and utilized in the next step of the data analysis. The NCI analysis was performed with the *Multiwfn* software (Version 3.6; Lu *et al.*, 2012). The analysis was performed for the direct crystallographic structures of the Cd complexes and for their DFT-optimized coun-

terparts. The electron densities of the former were calculated during a Single Point Energy calculation job type [M-11L/def2SV(P), without geometry optimization], while for the latter, they were calculated at the optimization step. Although, in the first case, electron densities were calculated without any optimization step, these results were used to compare how both experimental and DFT-optimized structures differed or not. The number of visualization points was 27×10^6 or higher. Such a large number provided a clear and unscattered weak interaction picture in each case. The *VMD* molecular visualization program (Version 1.9.2) was used for visualization of the NCI results (Humphrey *et al.*, 1996). For better clarity, these interactions were excluded from the results, according to the *Multiwfn* manual, and only Cd–ligand or ligand–ligand interactions were visualized.

2.5. Antimicrobial activity

The preliminary examination of the antifungal activity of compound **1** was performed with the microdilution plate method. RPMI 1640 supplemented with glucose and 3-(*N*-morpholino)propanesulfonic acid (MOPS) at a final concentration of 0.165 mol l^{-1} and pH 7.0 was applied as a culture medium. 18 isolates of fungi from the collection of the Department of Molecular Biotechnology and Microbiology were examined, *i.e. Alternaria alternata*, *Aspergillus flavus*, *A. fumigatus*, *A. niger*, *Candida albicans*, *C. catenulata*, *C. haemulonii*, *C. glabrata*, *C. kefyr*, *C. krusei*, *C. parapsilosis*, *C. tropicalis*, *C. utilis*, *Fusarium oxysporum* and *F. solani*, and the three dermatophyte isolates *Epidermophyton floccosum*, *Microsporum canis* and *Trichophyton rubrum*. All of the isolates were identified by conventional and molecular identification prior to deposition in the collection. The inoculum was prepared by suspending one colony from Sabouraud agar in 3 ml of distilled water. The inoculum was ready after the density reached 0.5 according to the McFarland standard, which is equal to 1–5 $\times$ 10^6 CFU ml^{-1}. 100 µl of the suspension was transferred to each well of columns 1–9 of the microdilution plate with 100 µl twofold dilutions of compound **1** (ranging from 4 to 0.016 mg l^{-1}). The wells in column 10 containing methanol were designed to exclude its influence, as **1** was dissolved in methanol. The wells in column 11 containing 100 µl of sterile drug-free medium containing pure inoculum served as the positive and sterility controls, and the wells in column 12 not containing inoculum served as the negative control. The microdilution plates were incubated for 24 h at 37 °C. The results were judged by eye after 24 h. The lowest concentration of **1** giving any inhibition of growth was regarded as the MIC value.

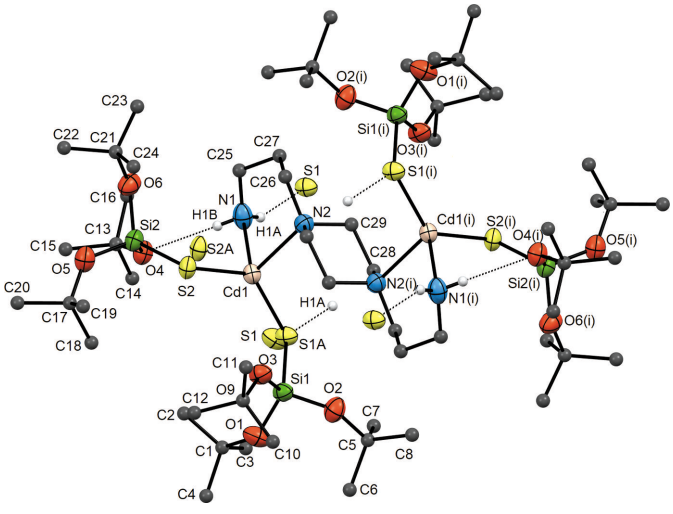

Figure 1
A fragment of the crystal structure of **1**, showing the environments of the metal centres, the atom-labelling scheme for the asymmetric unit and weak hydrogen bonding (as dashed lines). Displacement ellipsoids are drawn at the 50% probability level and the H atoms of the *tert*-butyl groups and of the BAAP ligand bonded to C atoms have been omitted for clarity. [Symmetry code: (i) $-x + 2, -y + 1, -z + 1$.]

3. Results and discussion

3.1. Synthesis

We have examined the coordination abilities of 1,4-bis(3-aminopropyl)piperazine (BAPP) in reactions with Cd^{II} tri-*tert*-butoxysilanethiolate, $[Cd\{SSi(OtBu)_3\}_2]_2$, under atmospheric conditions. At first, we combined $[Cd\{SSi(OtBu)_3\}_2]_2$ with BAPP in a molar ratio of 1:4 in methanol. The reaction yielded colourless crystals of dinuclear $[Cd_2\{SSi(OtBu)_3\}_4(\mu\text{-BAPP})]$, **1**, isolated after several days of crystallization at 4 °C (Scheme 1). The reaction of $[Cd\{SSi(OtBu)_3\}_2]_2$ with BAPP at the same molar ratio but in a toluene–methanol solvent system also yielded a colourless precipitate of the polynuclear compound $[Cd\{SSi(OtBu)_3\}_2(\mu\text{-BAPP})]_n$, **2**, which was further recrystallized from toluene at low temperature (−20 °C). After two weeks, colourless crystals of **2** suitable for X-ray analysis were obtained (Scheme 1). To check whether the solvent for the recrystallization influences the final structure of the product, we recorded ^{1}H NMR spectra for the precipitate obtained before recrystallization. The results clearly indicate that there are no free ligands in the precipitated product of the reaction before recrystallization (Figs. S1–S4 in the supporting information). Thus, one can assume that the use of toluene is crucial for obtaining polynuclear complex **2**. The obtained compounds were synthesized in fairly high yields and were stable under atmospheric conditions, enabling further tests to be carried out to determine their physicochemical properties.

3.2. Crystal structures

X-ray analysis results have shown that complexes **1** and **2** crystallize in the monoclinic space group $P2_1/n$. Complex **1** is dinuclear with metallic centres connected *via* the molecule of BAPP, which acts as a tetradentate bridging ligand and leads to the formation of a dimeric compound (Fig. 1 and Fig. S5 in supporting information). Each of the Cd^{II} atoms in compound **1** is chelated by two N atoms, *i.e.* one from the BAPP ring and the second from the amine group of the aminopropyl residues. The tetrahedral coordination sphere of each Cd^{II} atom is completed by two tri-*tert*-butoxysilanethiolate residues acting as *S*-donor terminal ligands.

The bond angles around the Cd^{II} atoms are in the range 88.42 (11)–135.39 (13)° (Table S1), indicating the presence of slight deviations from tetrahedral geometry, which was confirmed by the values of the structural parameters τ_4 and τ_4' (0.77 and 0.70, respectively) (Fig. S7) (Yang *et al.*, 2007; Okuniewski *et al.*, 2015; Rosiak *et al.*, 2018). However, these deviations do not affect the Cd—S bond lengths, while one of the Cd—N bonds is slightly longer when compared to those observed in other cadmium(II) silanethiolates with a tetrahedral metallic centre (Table S2) (Dołęga *et al.*, 2006, 2007; Pladzyk *et al.*, 2013, 2015; Kowalkowska *et al.*, 2017; Maślewski *et al.*, 2017). The molecule of **1** is centrosymmetric, with the inversion centre located in the middle of the piperazine ring of the BAPP molecule. The duplication of the asymmetric unit of complex **1** by this centre generates the second part of the dimer.

BAPP molecules are involved in the formation of hydrogen bonds, *i.e.* intramolecular N1(BAPP)—H1*B*···O4(TBST) [$D\cdots A$ = 3.115 (4)Å] and intermolecular N1(BAPP)—H1*A*···S1(TBST) [$D\cdots A$ = 3.519 (5) Å]. The parameters of these interactions are presented in Table S3. The presence of these intermolecular interactions causes the individual molecules of compound **1** to be interconnected and form one-dimensional chain structures through R_2^2 rings that join neighbouring molecules (Bernstein *et al.*, 1995). The distances between the Cd^{II} atoms in the molecule of **1** and the distances to the metallic centres of neighbouring molecules are almost identical at 6.3474 (6) and 6.3324 (6) Å, respectively.

Compound **2** is a polynuclear complex with a polymeric structure (Fig. 2 and S6). As in complex **1**, each Cd^{II} atom is coordinated by two S atoms from TBST residues and two N atoms from the RNH_2 groups of two BAPP bridging ligands that connect adjacent metallic centres.

The Cd—N and Cd—S bond lengths observed in **2** are similar to those found in other heteroleptic cadmium(II) silanethiolates (Table S1) (Dołęga *et al.*, 2006, 2007; Pladzyk *et al.*, 2013, 2015; Kowalkowska *et al.*, 2017; Maślewski *et al.*, 2017), whereas the angles at the Cd^{II} atoms range from 99.26 (10) to 120.28 (3)°. This indicates the presence of even smaller deviations from ideal tetrahedral geometry compared to complex **1** (τ_4 = 0.91 and τ_4' = 0.88) (Fig. S8 and Table S2) (Yang *et al.*, 2007; Okuniewski *et al.*, 2015; Rosiak *et al.*, 2018). Coordination polymer **2** is also centrosymmetric, with an inversion centre located at the middle of the six-membered piperazine ring of BAPP. The distances between the nearest Cd^{II} atoms within a single chain are 10.222 (2) and 11.424 (2) Å, while the distances between atoms belonging to neighbouring chains are shorter at 8.949 (2) and 9.677 (3) Å. The spatial arrangement of the polymeric chains of **2** enables the formation of diverse intramolecular interactions. Atoms N1 and N3 of the amino groups of the BAPP molecules are donors of two types of hydrogen-bonding interactions (Fig. 2). The first type is N(BAPP)—H···N(BAPP ring), between the amino group and an N atom belonging to the piperazine ring from the same BAPP ligand, *i.e.* N1—H1*A*···N2 [$D\cdots A$ = 2.977 (4) Å], as well as N3—H3*A*···N4 [$D\cdots A$ = 2.996 (4) Å]. The second type is the N(BAPP)—H···O(TBST) hydrogen-bonding interaction between the same amino group and the O atom of the silanethiolate residue, *i.e.* N1—H1*B*···O3 [$D\cdots A$ = 3.200 (4) Å] (Table S3). In addition, atom N1 is a donor in the next interaction, N1—H1*B*···O1, with the O atom of the TBST residue as the acceptor, so that the H1*B* atom is engaged in the formation of a three-centred hydrogen bond. The crystal packing of **2** shows that the polymer chains are arranged parallel to each other with no further significant interactions.

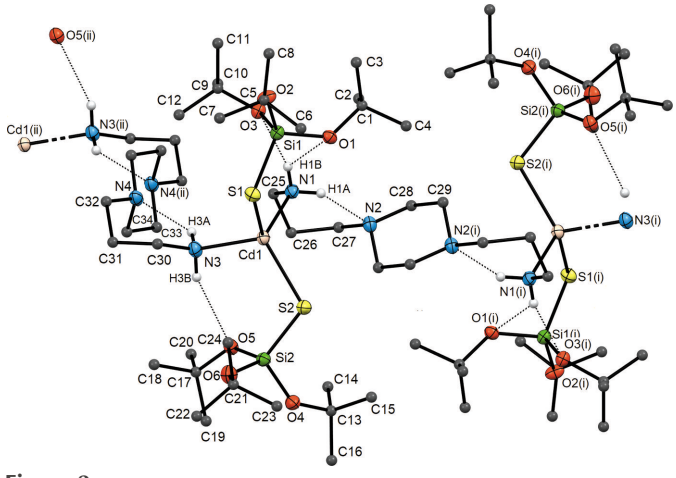

Figure 2
A fragment of the crystal structure of **2**, showing the environments of the metal centres, the atom-labelling scheme for the asymmetric unit and weak hydrogen bonding (as dashed lines). Displacement ellipsoids are drawn at the 50% probability level and the H atoms of the *tert*-butyl groups and of the BAAP ligand bonded to C atoms have been omitted for clarity. [Symmetry codes: (i) $-x+1, -y, -z+1$; (ii) $-x+1, -y+1, -z+1$.]

3.3. FT–IR spectroscopy

The FT–IR spectra were recorded for both complexes in the solid state (Fig. S9 in the supporting information). They are consistent with the crystal structures and confirm the presence of the ligands used in the syntheses (Nakamoto, 1997). The spectra of **1** and **2** contain bands of various intensities in the range from 3161 to 2675 cm^{-1}, characteristic for the symmetric and asymmetric vibrations of the C—H bonds of the methylene groups of BAPP, as well as the methyl groups present in the TBST residues. The number of bands occurring in this range for compound **2** is greater than for complex **1**. The bands observed in the range 1100–980 cm^{-1} for both complexes are characteristic for the Si—O—C bonding present in the $(t\mathrm{BuO})_3\mathrm{SiS}^-$ residues, and their patterns are typical for silanethiolate residues coordinating to metallic centres as terminal *S*-donor residues (Pladzyk *et al.*, 2021).

The BAPP ligand may be identified by the presence of the N—H symmetric and asymmetric stretching vibrations present at about 3330 cm^{-1} (3332 and 3257 cm^{-1} for **1**, and 3293 and 3232 cm^{-1} for **2**), the N—H deformation at 1584 and 1590 cm^{-1} for **1** and **2**, respectively, as well as the in-plane and out-of-plane N—H vibrations in the ranges 1480–1440 (1481 cm^{-1} for **1**, and 1492, 1458, and 1449 cm^{-1} for **2**) and 800–780 cm^{-1}, respectively. Other peaks typical for cyclic

amines are present at 1266, 1238 and 1204 cm^{-1} for **1**, and at 1263, 1251 and 1240 cm^{-1} for **2**, and correspond to C—N vibrations (Prabavathi *et al.*, 2015).

The def2sv(p) functional was applied in *GAUSSIAN16* (Frisch *et al.*, 2016) for the calculation of the FT–IR spectra of **1** and **2**. A comparison of the experimental and calculated spectra was carried out, together with assignments of the important features concluded from calculations (Table S4 and Fig. S10). Both the experimental and theoretical IR spectra are remarkably consistent. Virtually all vibrations in the experimental spectra can be assigned with the help of the calculated spectra, which confirms that the synthesis of both compounds was successful. Although no IR scale factor for the M11-L/def2sv(p) level of theory was found in the literature, it can be estimated as 0.92–0.93 on the basis of the N—H stretching bands, and mainly concerns higher wavenumber bands (about 3000 cm^{-1}).

The main difference between the experimental spectra of **1** and **2** is the additional N—H stretching band in **2**. This phenomenon is also reflected in the theoretical spectra. The reason for this is the inequality of various parts of the BAPP molecule in **2** (see Section 3.4). The inequality of the environments of the BAPP end groups in **2** allows for distinguishable differences in the N—H bond energies and vibration frequencies. Meanwhile, in **1**, both ends of the molecule interact symmetrically with two cadmium centres, *i.e.* they are equal or almost similar in energy and frequency.

3.4. NCI analysis of 1 and 2

The optimization step of the DFT calculations slightly altered the geometry of the initial complexes, and the overall structures of the crystallographic and optimized complexes were very similar. NCI interaction sites were initially determined for both the crystallographic and the DFT-optimized structures of complexes **1** and **2** within 1 nm of the Cd atom to verify if the crystallographic structure could be used directly in the qualitative NCI analysis. The optimized structures exhibited virtually all the interaction sites and properties present in the crystallographic structures; thus, the NCI analysis was performed for the real crystallographic structures. The IR spectra were derived from the optimized structures of both complexes.

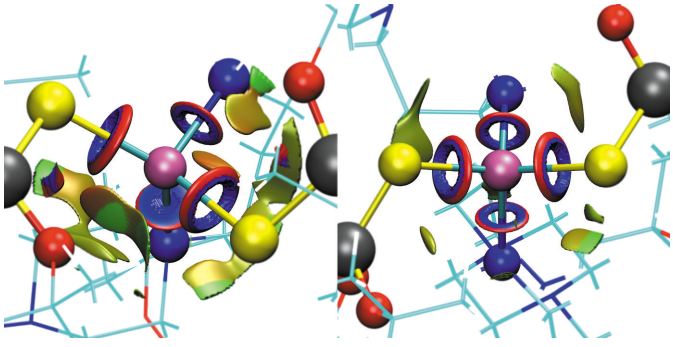

Figure 3
Weak interactions in the vicinity of the Cd atom as a result of the NCI analysis, with **1** on the left and **2** on the right. Green/olive irregular patches denote weak van der Waals-type interactions, while blue/red disks or rings denote relatively strong direct coordination interactions.

Usually, NCI analysis gives information on the type and strength of a weak bond. In this group of interactions, hydrogen bonds are considered the strongest visible in the NCI analysis results and are usually depicted as well-defined blue disks, according to the convention of the *Multiwfn* software and the developers of the method (Lu *et al.*, 2012). The disk shape reveals its directionality and the darker the blue colour, the stronger the bond. It should be noted that most Cd coordination bonds are stronger than an average hydrogen bond and NCI analysis indicates them not as blue disks (as for strong hydrogen bonds), but as blue/red rings. The hollow centre of such visualizations indicates that their classification as generally weak noncovalent interactions is barely justified.

3.4.1. Weak interactions in the vicinity of Cd. The neighbourhoods of the Cd atoms in **1** and **2** are strikingly different (see Fig. 3). These differences may be directly recognizable in these structures, yet NCI results aid in fully understanding them. The four main interaction sites in **2** are highly symmetrical. Both N—Cd sites are strong and energetically very similar, which is reflected in their almost identical shape and colour of the interaction indicator (blue/red ring). The same can be said for the S—Cd interactions. The overall environment of the Cd centre is open and accessible for other possible interactions.

Meanwhile, the N—Cd or S—Cd interactions in **1** are not equal. In particular, one of the N—Cd interactions turns out to be significantly weaker than the analogous interaction in **2** (full blue/red disk between Cd and N). The symmetry of the interactions is broken in comparison to **2**, probably due to the fact that both N—Cd interactions come from a single BAPP molecule, *i.e.* three molecules contribute to four Cd interactions. In the case of **2**, all four Cd coordination interactions are formed by four different molecules, which allows for more freedom in the spatial orientation of the ligand sites and is closer to the tetrahedral coordination of Cd.

The overall contribution of the van der Waals interactions (green/olive patches) in the case of **1** is significantly higher. The Cd atom in this complex is densely covered with other atoms of the structure, leaving no place for other inter- or intramolecular interactions. In particular, the spatial orientation of S—Si—O allows for weak O—Cd interactions in **1** (green patches between Cd and O), which is not possible in **2**. Most probably, these interactions are possible due to the inequality of the N—Cd interactions and the greater deviation of the Cd interaction distribution from the optimal tetrahedral orientation.

3.4.2. Weak interactions of 1,4-bis(3-aminopropyl)piperazine (BAPP). The better packing of **1** is also reflected in the number of interactions with the BAPP ligand. A visual inspection of the NCI results (see Figs. S11–S14 in the supporting information), focused this time on intermolecular interactions of the ligand with the rest of the structures of **1** or **2**, gives the impression that tightly organized complex **1** takes advantage of almost all possible intermolecular interactions involving Cd and the BAPP and TBST ligands. Van der Waals

interactions are numerous and relatively large in **1**, while in **2**, a scattered pattern of these weak interactions is revealed (in both possible variants of the ligand). Even though all interactions other than N—Cd are weak, their co-operativity should make the structure of **1** much more stable and stronger than that of **2**.

Moreover, weak but well-oriented C—H hydrogen bonds, symbolized by small green disks in the axis of C—H bonds, may play a significant role in the maintenance of the densely packed crystal structure. Eight such interactions can be spotted in the case of the BAPP fragment in **1**, while only two such directional interactions can be recognized in both variants of the ligand in **2**.

It can be argued that these kinds of interactions in **1** can be called true hydrogen bonds, yet such a directional and in-axis character, supported by a relatively large number per BAPP molecule, makes them stronger anyway.

3.5. Luminescence

The solid-state luminescence properties of powder samples of **1** and **2**, together with the free BAPP ligand and [Cd{SSi(O*t*Bu)$_3$}$_2$]$_2$, were investigated at ambient temperature. The entire spectroscopic study was carried out under identical experimental conditions. The optical absorption spectra of **1** and **2** have been measured by diffuse-reflectance experiments (see Fig. S15). The diffuse-reflectance spectra show two sharp absorption bands in the UV region at 226 and 257 nm for **1**, and at 225 and 252 nm for **2**, with a weaker signal region at 280–380 nm. The observed bands in this region of the prepared compounds can be assigned to electronic transitions from the ground-state S_0 level to the excited-state S_n levels of the BAPP piperazine ligand. The diagram of the energy levels for complexes [pipH]$_2$[Co(NCS)$_4$] and [pipH]$_2$[Ni(NCS)$_4$] (where pip is piperazine) has been proposed by Bie *et al.* (2005). Emission spectra were then recorded using these specific ultraviolet wavelengths (Fig. S16). In the case of **1**, a weak emission was observed, with a maximum located at about 350 nm, whereas in the case of **2**, week emissions located at about 350 and 420 nm were observed. This shows that excitation of the systems to the highest excited levels results in low emission intensities caused by large energy losses due to efficient non-radiative transitions to lower excited levels, from where emission takes place (Bie *et al.*, 2005).

Irradiation of all the systems with ultraviolet light in the solid state, monitoring the resulting emission at around 420 nm, was performed in order to determine the wavelength causing the greatest emission intensity. The excitation and emission spectra for the free BAPP ligand and compounds **1** and **2** are depicted in Fig. 4. Fig. 4(*a*) presents two excitation peaks of almost equal intensities (340 and 366 nm) for the free BAPP ligand. Upon incorporation of the BAPP ligand with Cd^{II} ions, excitations are observed at 346 and 370 nm for compound **1**, and at 360 nm for compound **2**. The maximum luminescence of the BAPP ligand is observed at 423 and 446 nm upon excitation at λ_{ex} = 366 nm, which corresponds to a blue luminescence. The shapes of the emission spectra of **1** and **2** are similar to the free BAPP emission. As seen in the figure, upon excitation at 346 nm, complex **1** exhibited weak emission peaks at 431 and 453 nm, which showed a small red shift of about 8 nm compared with the BAPP ligand. As in the case of the BAPP ligand, complex **2** shows a strong blue luminescence, with the main peaks at 418 and 439 nm, at an excitation wavelength of 360 nm. Unlike complex **1**, these emission bands are blue-shifted relative to the bands observed for the BAPP ligand. Broadband blue emission has been successfully realized in [pipH]$_2$[Co(NCS)$_4$] and [pipH]$_2$[Ni(NCS)$_4$] (Bie *et al.*, 2005), [Hg(μ_2-*L*H)Cl$_2$]$_2$[Hg$_2$(μ_2-Cl)$_2$Cl$_4$]·2H$_2$O and [Hg$_4$(μ_3-*L*)$_2$(μ_2-Cl)$_2$Cl$_6$] [*L* is *N*-(2-aminoethyl)piperazine] (Li *et al.*, 2007), [(N-AEPz)ZnCl$_4$]Cl (N-AEPz is *N*-aminoethylpiperazine) (Zhang *et al.*, 2020), (CuI)$_2$(*N*,*N*′-diethylpiperazine) (Safko *et al.*, 2012), (CuCN)$_2$(Pip) and (CuCN)$_2$(Me$_2$Pip) (Me$_2$Pip is *N*,*N*′-dimethylpiperazine) (Lim *et al.*, 2008), Ag(*L*)(ReO$_4$) [*L* is *N*-(2-aminoethyl)piperazine] (Kovalev *et al.*, 2015) and {[Cd(C$_4$H$_{11}$N$_2$)(μ-Cl)$_2$Cl]·H$_2$O}$_n$ (Mabrouk *et al.*, 2015). According to an earlier report, the free

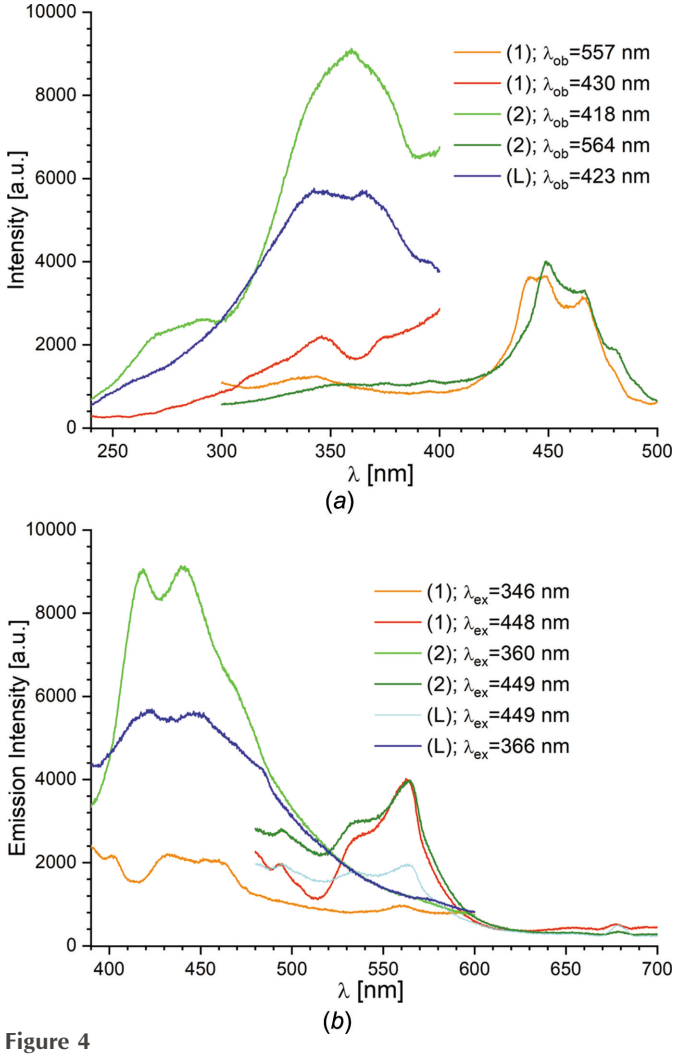

Figure 4
Room-temperature solid-state (*a*) excitation and (*b*) emission spectra of the BAPP ligand and compounds **1** and **2**.

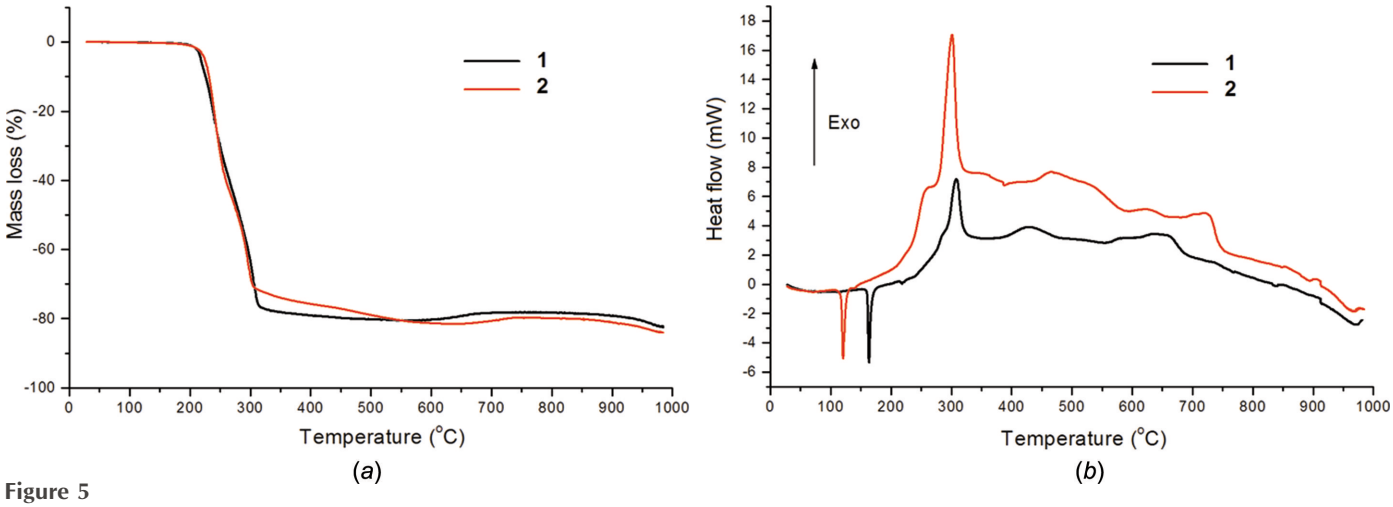

Figure 5
Thermal analysis of complexes **1** and **2** in air, showing (*a*) the TG curves and (*b*) the DSC curves.

piperazine ligand has an emission band at 418 nm on excitation at 312 nm (Bie *et al.*, 2005).

The BAPP luminescence emission position is red-shifted to 534 nm upon excitation at 449 nm and is accompanied by the appearance of a green luminescence (Fig. 4). In comparison with the blue luminescence, the green luminescence is characterized by its low intensity. Under 448 nm irradiation, complex **1** displayed a green emission with a peak at 562 nm. When **2** was excited at 449 nm, the luminescence spectrum exhibited an emission peak centred at 565 nm. However, compared to the BAPP ligand, the corresponding emission bands of compounds **1** and **2** have higher emission intensities. Considering the energy diagram proposed by Bie *et al.* (2005), the observed green emission is probably the result of a radiative transition from the lowest excited state of the ligand to its ground-state level.

Admittedly, the TBST residue present in **1** and **2** contains an Si—S bond where both elements have vacant 3*d* orbitals and, as a result, may participate in the emission process. Previous theoretical studies of the protonation and deprotonation of tri-*tert*-butoxysilanethiol using DFT and natural bond orbital (NBO) calculations have shown that lone pairs from sulfur in Si—S bonds are delocalized due to interaction with the antibonding σ*Si–O orbitals (Chojnacki, 2008*a*,*b*). Also, because of the polarization effects, these orbitals are strongly positioned on the silicon side. Therefore, the Si—S bonds are unlikely to condition the occurrence of emissions of complexes **1** and **2**. To confirm this, we conducted an additional experiment to determine whether the starting substrate $[Cd\{SSi(OtBu)_3\}_2]_2$ exhibits emission when excited and we observed no emission. Thus, we can assume that the luminescence differences between the emission properties of **1** and **2** (red and blue shifts relative to BAPP, and different intensities of their emission bands) should be attributed to their different structures, as shown by the X-ray studies.

3.6. Thermal analysis

The thermal behaviour of **1** and **2** was investigated simultaneously by TG–DSC (thermogravimetry–differential scanning calorimetry) and TG–FT–IR (thermogravimetry–Fourier transform infrared) methods. The cadmium complexes show different thermal stabilities under an air atmosphere. The dimeric complex **1** exhibits slightly lower thermal stability (177 °C) in comparison with polymeric complex **2** (187 °C). This observation can be explained in terms of their different crystal structures. In dimeric complex **1**, the Cd^{II} atoms are chelated by the amine ligand, forming a six-membered ring,

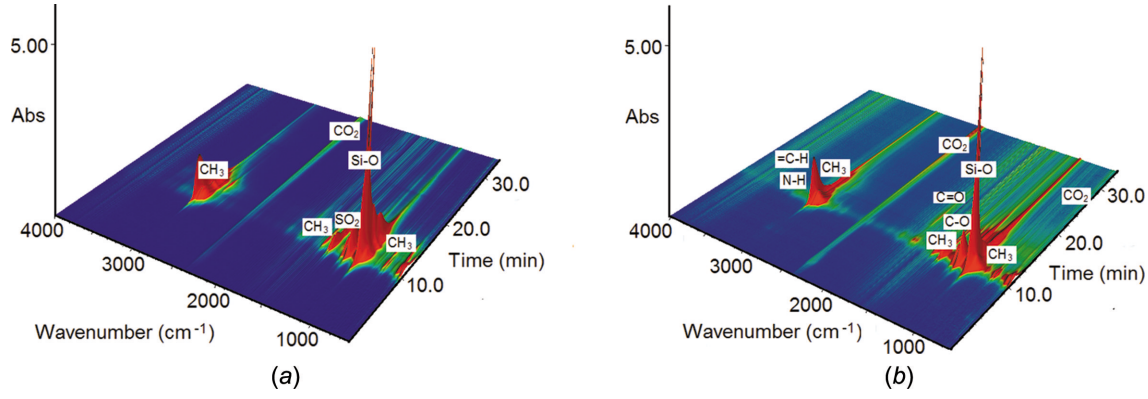

Figure 6
The FT–IR spectra of the evolved compounds during thermal decomposition of (*a*) **1** and (*b*) **2** under nitrogen.

which slightly reduces the thermal stability of the metal complex. The decomposition processes of both complexes [Fig. 5(*a*)] are preceded by the melting processes observed on the DSC curves [Fig. 5(*a*)].

The endothermic effects associated with melting were observed at 163.1 and 120.2 °C (peak tops) for **1** and **2**, respectively. Further heating results in the decomposition of the complexes connected with the significant mass losses observed on the TG curves. The mass losses of 76.50 (for **1**) and 70.41% (for **2**) were found in the relatively narrow temperature ranges of 188–317 and 151–308 °C. A detailed analysis of the DSC curve of **1** allows, in the above temperature range, a very weak endothermic effect to be distinguished at 217 °C (peak top). The DSC curves of both complexes are dominated by strong exothermic effects, with a maximum at about 300 °C [Fig. 6(*a*)]. These effects can be attributed to the burning processes of the organic parts of the cadmium complexes. Further heating of the solid residues causes some mass changes connected with their transformations [Fig. 6(*a*)]. The above-mentioned distinct mass losses point most probably to the formation of cadmium thiosilicate (Cd_2SiSO_3). At higher temperatures, further mass losses of 3.50 (for **1**) and 10.45% (for **2**) are observed. Taking into account that these mass changes were accompanied by exothermic effects, it can be assumed that the S atom of thiosilicate was oxidized and that the transformation of Cd_2SiSO_3 into Cd_2SiO_4 took place (Su *et al.*, 2018). Cadmium silicate is thermally stable in the temperature range 730–850 °C and, next, its further transformation takes place with the probable formation of cadmium oxide and silica (Kropidłowska *et al.*, 2007). The total observed mass losses recorded at 1000 °C for **1** and **2** were 82.42 and 84.00%, respectively.

Under a nitrogen atmosphere, the thermal decomposition of both compounds occurs above 160 °C. The TG curves exhibit significant mass losses of 81.3 and 82.0% up to 300 °C for **1** and **2**, respectively. The total recorded mass loss at 700 °C was 85% for both metal complexes. The solid residues of the cadmium complexes heated under an inert atmosphere are composed of some unidentified cadmium compounds and unburnt carbon species.

The FT–IR spectra of the gaseous products of the thermal decomposition of the metal complexes are dominated by bands derived from the evolved Si–alkoxy and *tert*-butyl compounds (Fig. 6). A very strong band at 1070 cm^{-1} was assigned to the stretching vibrations of the Si—O groups. The several bands with the strongest maxima at 2980 and 2942 cm^{-1}, as well as those at 1457 cm^{-1}, can be ascribed to the stretching and deformation vibrations of the methyl groups from the evolved moieties. The band at 1188 cm^{-1} can be assigned to the stretching vibrations of the C—O group from the tertiary alcohol molecules (Holly *et al.*, 1975; Silverstein & Webster, 1996). Breaking of the Si—S bonds in the molecules of the investigated cadmium complexes leads to the evolution of sulfur dioxide, which gives diagnostic double bands at 1390 and 1367 cm^{-1} (Łyszczek *et al.*, 2015). Heating of the complexes under an inert atmosphere also leads to the evolution of aliphatic hydrocarbons as a result of degradation of the coordinated amine group. The presence of bands in the regions 3000–2700 and 1480–1360 cm^{-1}, as well as those at 860 and 821 cm^{-1}, due to stretching, deformation and rocking vibrations of methyl groups, can indicate the evolution of the ethane/propane molecules. The IR spectra of complex **2** shows a broad weak band in the region 3200–3000 cm^{-1}, with a maximum at 3080 cm^{-1}, and a medium intensity band at 1277 cm^{-1}, which can be ascribed to the C—H, ═C—H and C—N stretching vibrations of some aliphatic amines and/or alkenes (Holly *et al.*, 1975; Silverstein & Webster, 1996). The formation of volatile species containing carbonyl groups (C═O) during the thermal decomposition of **2** is postulated based on the presence of a band at 1773 cm^{-1}. The FT–IR spectra of volatile compounds recorded above 400 °C also show relatively weak bands at 2341/2341 and 689 cm^{-1} from stretching and deformation vibrations of carbon dioxide molecules. It is worth mentioning that the intensity of CO_2 evolution is greater for compound **2** (Fig. 6).

3.7. Antimicrobial activity

The effective concentration of complex **1** was checked from 4 to 0.016 mg l^{-1}. The performed susceptibility tests exhibited a lack of antifungal activity of **1** against 14 of the tested isolates, but for three tested dermatophytes, *i.e. Epidermophyton floccosum*, *Microsporum canis* and *Trichophyton rubrum*, the inhibition of their growth was observed at 0.25 mg l^{-1} and above. The mechanism of the toxicity of **1** towards the fungal isolates relies on Cd, however, the influence of other groups cannot be excluded thus far. Moreover, the fungal specimens are generally considered to be tolerant to heavy metals due to their presence in soil (Rajapaksha *et al.*, 2004; Bhajbhuje *et al.*, 2013; Li *et al.*, 2019). In the case of the influence of cadmium on the dermatophytes, there has been one report confirming its antifungal activity; however, the test was performed with the colony diameter method (Al-Janabi, 2011). This specific antifungal activity may also be related to the fact that the development and growth of dermatophytes depends strongly on keratin, a hydrophobic protein rich in sulfur-containing amino acids such as cysteine and methionine (Ciesielska *et al.*, 2021), which, being soft bases, have a particular affinity for soft acids like Cd^{2+} ions. To address the question of the antidermatophyte effect of **1**, further investigations are being considered.

4. Conclusion

In summary, this study has provided detailed insight into the structures of two new heteroleptic cadmium tri-*tert*-butoxysilanethiolates with 1,4-bis(3-aminopropyl)piperazine synthesized in different solvent systems while maintaining the remaining reaction conditions. The experiments yielded compounds with different structures and the absence of solvent molecules crystallizing in the structures. The structures of the obtained complexes appeared to be crucial for their spectral properties and antifungal activity. Compound **1** inhibits the growth of fungi belonging to the group of dermatophytes. The results of our study show that it is worth extending

the study to other metal silanethiolates with the purpose of obtaining compounds with better antimicrobial activity and luminescence.

Acknowledgements

The research was supported by the 'Excellence Initiative – Research University' programs at Gdańsk University of Technology and the Silicium Supporting Core R&D Facilities program (crystallographic measurements). Computations were carried out using the computers of Centre of Informatics Tricity Academic Supercomputer & Network.

Funding information

Funding for the crystallographic measurements was provided by: Gdańsk University of Technology (grant No. DEC-2/2021/IDUB/V.6/Si).

References

Al-Janabi, A. (2011). *Mycoses*, **54**, 345–349.
Bernstein, J., Davis, R. E., Shimoni, L. & Chang, N.-L. (1995). *Angew. Chem. Int. Ed. Engl.* **34**, 1555–1573.
Bhajbhuje, M. N. (2013). *Int. J. Life Sci.* **1**, 51–62.
Bie, H.-J., Lu, J., Yu, J.-H., Xu, J.-Q., Zhao, K. & Zhang, X. (2005). *J. Solid State Chem.* **178**, 1445–1451.
Buta, I., Nistor, M. A., Lönnecke, P., Hey-Hawkins, E., Muntean, S. G. & Costisor, O. (2021). *J. Photochem. Photobiol. Chem.* **404**, 112961–112970.
Chojnacki, J. (2008*a*). *J. Mol. Struct. Theochem*, **862**, 112–117.
Chojnacki, J. (2008*b*). *Polyhedron*, **27**, 969–976.
Ciesielska, A., Kawa, A., Kanarek, K., Soboń, A. & Szewczyk, R. (2021). *Sci. Rep.* **11**, 3959–3969.
Dołęga, A., Baranowska, K., Gajda, J., Kaźmierski, S. & Potrzebowski, M. J. (2007). *Inorg. Chim. Acta*, **360**, 2973–2982.
Dołęga, A., Godlewska, S. & Baranowska, K. (2006). *Acta Cryst.* E**62**, m3567–m3569.
Dolomanov, O. V., Bourhis, L. J., Gildea, R. J., Howard, J. A. K. & Puschmann, H. (2009). *J. Appl. Cryst.* **42**, 339–341.
Farrugia, L. J. (2012). *J. Appl. Cryst.* **45**, 849–854.
Frisch, M. J., Trucks, G. W., Schlegel, H. B., Scuseria, G. E., Robb, M. A., Cheeseman, J. R., Scalmani, G., Barone, V., Petersson, G. A., Nakatsuji, H., Li, X., Caricato, M., Marenich, A. V., Bloino, J., Janesko, B. G., Gomperts, R., Mennucci, B., Hratchian, H. P., Ortiz, J. V., Izmaylov, A. F., Sonnenberg, J. L., Williams-Young, D., Ding, F., Lipparini, F., Egidi, F., Goings, J., Peng, B., Petrone, A., Henderson, T., Ranasinghe, D., Zakrzewski, V. G., Gao, J., Rega, N., Zheng, G., Liang, W., Hada, M., Ehara, M., Toyota, K., Fukuda, R., Hasegawa, J., Ishida, M., Nakajima, T., Honda, Y., Kitao, O., Nakai, H., Vreven, T., Throssell, K., Montgomery, J. A. Jr, Peralta, J. E., Ogliaro, F., Bearpark, M. J., Heyd, J. J., Brothers, E. N., Kudin, K. N., Staroverov, V. N., Keith, T. A., Kobayashi, R., Normand, J., Raghavachari, K., Rendell, A. P., Burant, J. C., Iyengar, S. S., Tomasi, J., Cossi, M., Millam, J. M., Klene, M., Adamo, C., Cammi, R., Ochterski, J. W., Martin, R. L., Morokuma, K., Farkas, O., Foresman, J. B. & Fox, D. J. (2016). *GAUSSIAN16*. Gaussian Inc., Wallingford, CT, USA. https://gaussian.com/.
Gennari, M. & Duboc, C. (2020). *Acc. Chem. Res.* **53**, 2753–2761.
Guillon, J., Cohen, A., Gueddouda, M., Das, R. N., Moreau, S., Ronga, L., Savrimoutou, S., Basmaciyan, L., Monnier, A., Monget, M., Rubio, S., Garnerin, T., Azas, N., Mergny, J.-L., Mullié, C. & Sonnet, P. (2017). *J. Enzyme Inhib. Med. Chem.* **32**, 547–563.
Henkel, G. & Krebs, B. (2004). *Chem. Rev.* **104**, 801–824.
Holly, S. & Sohar, P. (1975). In *Absorption Spectra in the Infrared Region*. Budapest: Akadémiai Kiadó.
Humphrey, W., Dalke, A. & Schulten, K. (1996). *J. Mol. Graph.* **14**, 33–38.
Keypour, H., Rezaeivala, M., Valencia, L. & Pérez-Lourido, P. (2008). *Polyhedron*, **27**, 3172–3176.
Keypour, H., Rezaeivala, M., Valencia, L., Pérez-Lourido, P. & Khavasi, H. R. (2009). *Polyhedron*, **28**, 3755–3758.
Korkola, N. C. & Stillman, M. J. (2023). *J. Am. Chem. Soc.* **145**, 6383–6397.
Kovalev, V. V., Gorbunova, Y. E., Kozyukhin, S. A. & Kokunov, Y. V. (2015). *Russ. J. Coord. Chem.* **41**, 332–337.
Kowalkowska, D., Dołęga, A., Nedelko, N., Hnatejko, Z., Ponikiewski, Ł., Matracka, A., Ślawska-Waniewska, A., Strągowska, A., Słowy, K., Gazda, M. & Pladzyk, A. (2017). *CrystEngComm*, **19**, 3506–3518.
Koziskova, J., Hahn, F., Richter, J. & Kozisek, J. (2016). *Acta Chim. Slovaca*, **9**, 136–140.
Kropidłowska, A., Strankowski, M., Gazda, M. & Becker, B. (2007). *J. Therm. Anal. Calorim.* **88**, 463–470.
Li, C., Zhou, K. & Qin, W. (2019). *Soil Sediment Contamin.* **28**, 380–394.
Li, J., Ding, B., Yang, E.-C., Wang, X.-G. & Zhao, X.-J. (2007). *Z. Anorg. Allg. Chem.* **633**, 346–350.
Lim, M. J., Murray, C. A., Tronic, T. A., deKrafft, K. E., Ley, A. N., deButts, J. C., Pike, R. D., Lu, H. & Patterson, H. H. (2008). *Inorg. Chem.* **47**, 6931–6947.
Lu, T. & Chen, F. (2012). *J. Comput. Chem.* **33**, 580–592.
Łyszczek, R., Ostasz, A., Bartyzel, A. & Lipke, A. (2015). *J. Anal. Appl. Pyrolysis*, **115**, 370–378.
Mabrouk, S. B., Dkhili, S., Besbes-Hentati, S., Derbel, N., Sbihi, H., Rzaigui, M. & Abid, S. (2015). *Res. Chem. Intermed.* **41**, 9871–9883.
Macrae, C. F., Sovago, I., Cottrell, S. J., Galek, P. T. A., McCabe, P., Pidcock, E., Platings, M., Shields, G. P., Stevens, J. S., Towler, M. & Wood, P. A. (2020). *J. Appl. Cryst.* **53**, 226–235.
Maślewski, P., Kazimierczuk, K., Hnatejko, Z. & Dołęga, A. (2017). *Inorg. Chim. Acta*, **459**, 22–28.
Nakamoto, K. (1997). In *Infrared and Raman Spectra of Inorganic and Coordination Compounds*, 5th ed. Hoboken, NY: Wiley.
Nemati, L., Keypour, H., Shahabadi, N., Hadidi, S. & William Gable, R. (2021). *J. Mol. Liq.* **337**, 116292–116304.
Niemeyer, H. M. (1979). *J. Mol. Struct.* **57**, 241–244.
Okuniewski, A., Rosiak, D., Chojnacki, J. & Becker, B. (2015). *Polyhedron*, **90**, 47–57.
Peverati, R. & Truhlar, D. G. (2012). *J. Phys. Chem. Lett.* **3**, 117–124.
Pladzyk, A., Baranowska, K., Dziubińska, K. & Ponikiewski, Ł. (2013). *Polyhedron*, **50**, 121–130.
Pladzyk, A., Kowalkowska-Zedler, D., Ciborska, A., Schnepf, A. & Dołęga, A. (2021). *Coord. Chem. Rev.* **437**, 213761–213834.
Pladzyk, A., Ponikiewski, Ł., Dołęga, A., Słowy, K., Sokołowska, A., Dziubińska, K. & Hnatejko, Z. (2015). *Chem. Asian J.* **10**, 2388–2396.
Półrolniczak, A., Sobczak, S. & Katrusiak, A. (2018). *Inorg. Chem.* **57**, 8942–8950.
Prabavathi, N., Nayaki, S. & Krishnakumar, V. (2015). *Pharm. Anal. Acta*, **6**, 391.
Ragab, M. S., Shehata, M. R., Shoukry, M. M., Haukka, M. & Ragheb, M. A. (2022). *RSC Adv.* **12**, 1871–1884.
Rajapaksha, R. M. C. P., Tobor-Kapłon, M. A. & Bååth, E. (2004). *Appl. Environ. Microbiol.* **70**, 2966–2973.
Resta, V., Laera, A. M., Piscopiello, E., Capodieci, L., Ferrara, M. C. & Tapfer, L. (2010). *Phys. Status Solidi A*, **207**, 1631–1635.
Rosiak, D., Okuniewski, A. & Chojnacki, J. (2018). *Polyhedron*, **146**, 35–41.
Ryckebusch, A., Deprez-Poulain, R., Maes, L., Debreu-Fontaine, M.-A., Mouray, E., Grellier, P. & Sergheraert, C. (2003). *J. Med. Chem.* **46**, 542–557.

Safko, J. P., Kuperstock, E., McCullough, S. M., Noviello, A. M., Li, X., Killarney, J. P., Murphy, C., Patterson, H. H., Bayse, C. A. & Pike, R. D. (2012). *Dalton Trans.* **41**, 11663–11674.
Sheldrick, G. M. (2015*a*). *Acta Cryst.* A**71**, 3–8.
Sheldrick, G. M. (2015*b*). *Acta Cryst.* C**71**, 3–8.
Silverstein, R. M. & Webster, F. X. (1996). In *Spectrometric Identification of Organic Compounds*, 6th ed. New York: Wiley.
Singh, M. K., Sutradhar, S., Paul, B., Adhikari, S., Butcher, R. J., Acharya, S. & Das, A. (2015). *J. Coord. Chem.* **68**, 1423–1432.
Stoe & Cie (2016). *X-AREA*. Version 1.75. Stoe & Cie GmbH, Darmstadt, Germany.
Su, M., Tang, J., Liao, Ch., Kong, L., Xiao, T., Shih, K., Song, G., Chen, D. & Zhang, H. (2018). *Environ. Pollut.* **239**, 571–578.
Weigend, F. & Ahlrichs, R. (2005). *Phys. Chem. Chem. Phys.* **7**, 3297–3305.
Wing-Wah Yam, V., Pui, Y.-L. & Cheung, K.-K. (1999). *New J. Chem.* **23**, 1163–1169.
Wojnowski, W., Becker, B., Walz, L., Peters, K., Peters, E. & von Schnering, H. G. (1992). *Polyhedron*, **11**, 607–612.
Yang, L., Powell, D. R. & Houser, R. P. (2007). *Dalton Trans.* pp. 955–964.
Zhang, X., Li, L., Wang, S., Liu, X., Yao, Y., Peng, Y., Hong, M. & Luo, J. (2020). *Inorg. Chem.* **59**, 3527–3531.

supporting information

Acta Cryst. (2023). C**79**, 305-315 [https://doi.org/10.1107/S2053229623005442]

Solvent influence on the crystal structures of new cadmium tri-*tert*-butoxysilanethiolate complexes with 1,4-bis(3-aminopropyl)piperazine: luminescence and antifungal activity

Daria Kowalkowska-Zedler, Piotr Bruździak, Zbigniew Hnatejko, Renata Łyszczek, Anna Brillowska-Dąbrowska, Łukasz Ponikiewski, Bartosz Cieśla and Agnieszka Pladzyk

Computing details

For both structures, data collection: WinXpose in *X-AREA* (Stoe & Cie, 2016); cell refinement: Recipe in *X-AREA* (Stoe & Cie, 2016); data reduction: Integrate and *X-RED32* in *X-AREA* (Stoe & Cie, 2016); program(s) used to solve structure: SHELXT2014 (Sheldrick, 2015*a*); program(s) used to refine structure: *SHELXL2018* (Sheldrick, 2015*b*); molecular graphics: *ORTEP-3 for Windows* (Farrugia, 2012) and *Mercury* (Macrae *et al.*, 2020); software used to prepare material for publication: *WinGX* publication routines (Farrugia, 2012) and OLEX2 (Dolomanov *et al.*, 2009).

***catena*-Poly[[bis(tri-*tert*-butoxysilanethiolato-κS)cadmium(II)]-μ-μ-1,4-bis(3-aminopropyl)piperazine-$\kappa^2N^{1'}$:$N^{4'}$] (dkz2)**

Crystal data

$[Cd(C_{12}H_{27}O_3SSi)_2(C_{10}H_{24}N_4)]$
M_r = 871.7
Monoclinic, $P2_1/n$
Hall symbol: -P 2yn
a = 16.424 (5) Å
b = 16.876 (4) Å
c = 18.265 (5) Å
β = 112.66 (2)°
V = 4672 (2) Å^3
Z = 4
$F(000)$ = 1864
D_x = 1.239 Mg m^{-3}
Mo $K\alpha$ radiation, λ = 0.71073 Å
Cell parameters from 42943 reflections
θ = 2.4–29.6°
μ = 0.65 mm^{-1}
T = 120 K
Prism, colorless
0.38 × 0.34 × 0.3 mm

Data collection

Stoe IPDS 2T diffractometer
Radiation source: GeniX Mo, 0.05 x 0.05 mm2 microfocus
Parabolic x-ray mirror monochromator
Detector resolution: 6.67 pixels mm^{-1}
rotation method, ω scans
Absorption correction: multi-scan [LANA (Koziskova *et al.*, 2016) and X-Red32 in X-AREA (Stoe & Cie, 2016)]
T_{min} = 0.664, T_{max} = 0.970
33547 measured reflections
9535 independent reflections
8345 reflections with $I > 2\sigma(I)$
R_{int} = 0.045
θ_{max} = 26.4°, θ_{min} = 2.4°
h = −20→20
k = −21→21
l = −22→22

Refinement

Refinement on F^2
Least-squares matrix: full
$R[F^2 > 2\sigma(F^2)] = 0.043$
$wR(F^2) = 0.107$
$S = 1.14$
9535 reflections
476 parameters
0 restraints
0 constraints

Hydrogen site location: mixed
H atoms treated by a mixture of independent and constrained refinement
$w = 1/[\sigma^2(F_o^2) + (0.0283P)^2 + 12.4766P]$ where $P = (F_o^2 + 2F_c^2)/3$
$(\Delta/\sigma)_{max} = 0.001$
$\Delta\rho_{max} = 1.32$ e Å^{-3}
$\Delta\rho_{min} = -0.74$ e Å^{-3}

Special details

Geometry. All esds (except the esd in the dihedral angle between two l.s. planes) are estimated using the full covariance matrix. The cell esds are taken into account individually in the estimation of esds in distances, angles and torsion angles; correlations between esds in cell parameters are only used when they are defined by crystal symmetry. An approximate (isotropic) treatment of cell esds is used for estimating esds involving l.s. planes.

Refinement. Single-crystal X-ray diffraction data of compounds **1** and **2** were collected at 120 (2) K with a Stoe IPDS-2T diffractometer equipped with a graphite-monochromated Mo *Kα* radiation source. Crystals were cooled using a Cryostream 800 open-flow nitrogen cryostat (Oxford Cryosystems). Data collection and image processing was performed with X-AREA 1.75 (Stoe & Cie, 2016). Intensity data were scaled with LANA (part of X-AREA) in order to minimize differences in intensities of symmetry-equivalent reflections (a multi-scan method). The structures of **1** and **2** were solved using intrinsic phasing procedure implemented in SHELXT and all non-hydrogen atoms were refined with anisotropic displacement parameters by full-matrix least squares procedure based on F^2 using the SHELX–2014 program package (Sheldrick, 2014; Sheldrick, 2015). The OLEX2 (Dolomanov *et al.*, 2009) and Wingx (Farrugia, 2012) program suites were used to prepare the final version of CIF files. Mercury (Macrae *et al.*, 2020) was used to prepare the figures.

Fractional atomic coordinates and isotropic or equivalent isotropic displacement parameters (Å²)

	x	*y*	*z*	U_{iso}*/U_{eq}
C1	0.8273 (2)	0.0825 (2)	0.5368 (2)	0.0258 (7)
C2	0.7506 (2)	0.1086 (2)	0.4622 (2)	0.0298 (8)
H2A	0.694784	0.096941	0.467831	0.045*
H2B	0.75269	0.080076	0.416299	0.045*
H2C	0.754765	0.165737	0.454563	0.045*
C3	0.9144 (3)	0.0959 (3)	0.5281 (3)	0.0449 (11)
H3C	0.921048	0.15231	0.519105	0.067*
H3D	0.915393	0.065177	0.48289	0.067*
H3E	0.962928	0.078726	0.576588	0.067*
C4	0.8171 (3)	−0.0047 (2)	0.5535 (2)	0.0392 (10)
H4A	0.866903	−0.021075	0.601462	0.059*
H4B	0.815997	−0.036777	0.508446	0.059*
H4C	0.761873	−0.012177	0.561413	0.059*
C5	1.0397 (2)	0.2144 (2)	0.7307 (2)	0.0276 (8)
C6	1.0337 (2)	0.1353 (2)	0.7682 (2)	0.0307 (8)
H6A	0.984744	0.136696	0.786217	0.046*
H6B	1.089016	0.125177	0.813563	0.046*
H6C	1.023566	0.092947	0.728917	0.046*
C7	1.0519 (3)	0.2821 (2)	0.7886 (2)	0.0440 (11)
H7A	1.05456	0.3323	0.762738	0.066*
H7B	1.106879	0.274397	0.834991	0.066*
H7C	1.002072	0.28319	0.805555	0.066*

C8	1.1147 (3)	0.2131 (3)	0.7022 (3)	0.0504 (12)
H8A	1.10501	0.170413	0.663437	0.076*
H8B	1.170454	0.204094	0.747422	0.076*
H8C	1.117281	0.264013	0.677378	0.076*
C9	0.8199 (2)	0.3511 (2)	0.5430 (2)	0.0246 (7)
C10	0.7397 (2)	0.3709 (2)	0.4687 (2)	0.0338 (8)
H10A	0.735276	0.332955	0.426703	0.051*
H10B	0.745763	0.424598	0.451106	0.051*
H10C	0.686349	0.367773	0.48042	0.051*
C11	0.9030 (2)	0.3560 (3)	0.5256 (2)	0.0367 (9)
H11A	0.954246	0.341715	0.573314	0.055*
H11B	0.910174	0.41016	0.50967	0.055*
H11C	0.898261	0.319272	0.482583	0.055*
C12	0.8261 (3)	0.4054 (2)	0.6105 (2)	0.0400 (10)
H12A	0.772479	0.400491	0.6215	0.06*
H12B	0.832473	0.46025	0.595916	0.06*
H12C	0.877505	0.390713	0.657914	0.06*
C13	0.3820 (2)	0.0780 (2)	0.7621 (2)	0.0276 (7)
C14	0.3326 (3)	0.1069 (3)	0.6770 (2)	0.0376 (9)
H14A	0.29846	0.154435	0.677512	0.056*
H14B	0.292574	0.065275	0.646035	0.056*
H14C	0.375102	0.11964	0.653084	0.056*
C15	0.4309 (3)	0.0022 (2)	0.7635 (3)	0.0435 (10)
H15A	0.4732	0.010954	0.73838	0.065*
H15B	0.388797	−0.039032	0.734411	0.065*
H15C	0.462507	−0.014772	0.818541	0.065*
C16	0.3172 (3)	0.0657 (3)	0.8029 (3)	0.0384 (9)
H16A	0.349078	0.045546	0.856713	0.058*
H16B	0.271919	0.027445	0.772557	0.058*
H16C	0.289188	0.116335	0.805485	0.058*
C17	0.4078 (2)	0.3344 (2)	0.7516 (2)	0.0267 (7)
C18	0.4680 (3)	0.3998 (2)	0.7996 (2)	0.0354 (9)
H18A	0.506218	0.379133	0.851693	0.053*
H18B	0.432303	0.443486	0.806606	0.053*
H18C	0.504369	0.419122	0.77162	0.053*
C19	0.3536 (3)	0.3027 (2)	0.7971 (3)	0.0419 (10)
H19A	0.314902	0.260064	0.766515	0.063*
H19B	0.317762	0.345616	0.805227	0.063*
H19C	0.393419	0.28214	0.848633	0.063*
C20	0.3478 (3)	0.3651 (3)	0.6702 (3)	0.0481 (11)
H20A	0.383771	0.383942	0.641646	0.072*
H20B	0.311806	0.40888	0.676548	0.072*
H20C	0.309089	0.322257	0.640025	0.072*
C21	0.6348 (2)	0.2116 (2)	0.9489 (2)	0.0289 (8)
C22	0.6266 (3)	0.2626 (3)	1.0138 (2)	0.0504 (12)
H22A	0.635215	0.318352	1.003503	0.076*
H22B	0.671545	0.246823	1.065081	0.076*
H22C	0.567847	0.255713	1.014838	0.076*

C23	0.6204 (3)	0.1257 (3)	0.9648 (3)	0.0525 (12)
H23A	0.562196	0.119827	0.967313	0.079*
H23B	0.666114	0.109211	1.015347	0.079*
H23C	0.623602	0.092573	0.921903	0.079*
C24	0.7221 (3)	0.2236 (5)	0.9424 (3)	0.077 (2)
H24A	0.728169	0.185755	0.904091	0.115*
H24B	0.769616	0.215035	0.994359	0.115*
H24C	0.725574	0.277721	0.924451	0.115*
C25	0.5395 (2)	0.2581 (2)	0.4966 (2)	0.0255 (7)
H25A	0.539003	0.259021	0.442257	0.031*
H25B	0.546612	0.313288	0.516516	0.031*
C26	0.4524 (2)	0.2256 (2)	0.4939 (2)	0.0312 (8)
H26A	0.406284	0.266468	0.47104	0.037*
H26B	0.457478	0.215052	0.548752	0.037*
C27	0.4231 (2)	0.1495 (2)	0.4452 (2)	0.0318 (8)
H27A	0.36341	0.135042	0.441904	0.038*
H27B	0.419297	0.159601	0.390558	0.038*
C28	0.4691 (2)	0.0206 (2)	0.4188 (2)	0.0271 (7)
H28A	0.479269	0.042621	0.372859	0.033*
H28B	0.407371	0.001508	0.399917	0.033*
C29	0.4686 (2)	0.0479 (2)	0.5464 (2)	0.0261 (7)
H29A	0.406893	0.029049	0.529066	0.031*
H29B	0.478062	0.088975	0.587529	0.031*
C30	0.6762 (3)	0.4103 (2)	0.7398 (2)	0.0300 (8)
H30A	0.732835	0.404701	0.73285	0.036*
H30B	0.68679	0.395558	0.795168	0.036*
C31	0.6472 (3)	0.4975 (2)	0.7267 (2)	0.0281 (8)
H31A	0.588634	0.502456	0.729971	0.034*
H31B	0.689433	0.529733	0.769959	0.034*
C32	0.6415 (3)	0.5314 (2)	0.6469 (2)	0.0281 (8)
H32A	0.628458	0.588781	0.645733	0.034*
H32B	0.699892	0.525678	0.643409	0.034*
C33	0.5841 (2)	0.5230 (2)	0.5043 (2)	0.0269 (7)
H33A	0.643792	0.509774	0.506718	0.032*
H33B	0.577936	0.581444	0.5017	0.032*
C34	0.4844 (2)	0.5131 (2)	0.5697 (2)	0.0265 (7)
H34A	0.476718	0.571311	0.568186	0.032*
H34B	0.475586	0.492749	0.617002	0.032*
Cd1	0.66166 (2)	0.22716 (2)	0.68348 (2)	0.01980 (7)
N1	0.61539 (19)	0.20993 (17)	0.54853 (17)	0.0213 (6)
N2	0.48273 (18)	0.08247 (16)	0.47839 (16)	0.0220 (6)
N3	0.6112 (2)	0.35403 (17)	0.68530 (18)	0.0240 (6)
N4	0.5745 (2)	0.49401 (16)	0.57640 (16)	0.0241 (6)
O1	0.82513 (14)	0.12462 (13)	0.60513 (12)	0.0200 (5)
O2	0.96109 (14)	0.22811 (14)	0.66101 (13)	0.0234 (5)
O3	0.80536 (14)	0.26968 (13)	0.56140 (13)	0.0199 (4)
O4	0.44271 (15)	0.13785 (14)	0.80805 (14)	0.0249 (5)
O5	0.46047 (15)	0.27295 (13)	0.73567 (13)	0.0243 (5)

O6	0.56721 (16)	0.23889 (15)	0.87650 (14)	0.0285 (5)
S1	0.82429 (5)	0.23320 (5)	0.73707 (5)	0.02238 (17)
S2	0.58603 (6)	0.13526 (5)	0.74087 (5)	0.02728 (19)
Si1	0.85637 (6)	0.21366 (5)	0.63890 (5)	0.01761 (18)
Si2	0.51154 (6)	0.19731 (5)	0.79140 (5)	0.02019 (18)
H1A	0.602 (3)	0.160 (3)	0.532 (2)	0.027 (10)*
H1B	0.661 (3)	0.220 (2)	0.540 (2)	0.026 (10)*
H3A	0.586 (3)	0.375 (2)	0.633 (3)	0.034 (11)*
H3B	0.563 (3)	0.348 (3)	0.698 (3)	0.040 (12)*

Atomic displacement parameters (Å²)

	U^{11}	U^{22}	U^{33}	U^{12}	U^{13}	U^{23}
C1	0.0277 (18)	0.0245 (17)	0.0218 (16)	0.0027 (14)	0.0057 (14)	−0.0044 (13)
C2	0.035 (2)	0.0280 (18)	0.0215 (16)	0.0048 (16)	0.0051 (15)	−0.0034 (14)
C3	0.033 (2)	0.066 (3)	0.039 (2)	0.000 (2)	0.0174 (18)	−0.017 (2)
C4	0.051 (2)	0.0242 (18)	0.032 (2)	0.0094 (18)	0.0044 (18)	−0.0050 (16)
C5	0.0164 (16)	0.0323 (19)	0.0258 (17)	−0.0030 (14)	−0.0009 (13)	0.0096 (14)
C6	0.0209 (17)	0.0304 (19)	0.0317 (19)	0.0011 (15)	0.0000 (14)	0.0098 (15)
C7	0.042 (2)	0.034 (2)	0.036 (2)	−0.0147 (19)	−0.0067 (18)	0.0014 (17)
C8	0.0166 (18)	0.083 (4)	0.049 (3)	0.002 (2)	0.0098 (17)	0.025 (2)
C9	0.0231 (16)	0.0236 (16)	0.0271 (17)	−0.0019 (14)	0.0097 (14)	0.0064 (14)
C10	0.0276 (19)	0.0315 (19)	0.037 (2)	0.0060 (16)	0.0063 (16)	0.0152 (16)
C11	0.0277 (19)	0.042 (2)	0.042 (2)	0.0026 (17)	0.0156 (17)	0.0162 (18)
C12	0.059 (3)	0.0252 (19)	0.036 (2)	0.0011 (19)	0.019 (2)	0.0027 (16)
C13	0.0247 (17)	0.0255 (17)	0.0349 (19)	−0.0063 (14)	0.0142 (15)	−0.0076 (15)
C14	0.035 (2)	0.042 (2)	0.033 (2)	−0.0111 (18)	0.0100 (17)	−0.0104 (17)
C15	0.042 (2)	0.0249 (19)	0.070 (3)	−0.0004 (18)	0.028 (2)	−0.0056 (19)
C16	0.035 (2)	0.038 (2)	0.050 (2)	−0.0088 (17)	0.0246 (19)	−0.0039 (18)
C17	0.0226 (16)	0.0237 (17)	0.0334 (18)	0.0040 (14)	0.0104 (14)	−0.0033 (14)
C18	0.035 (2)	0.0256 (18)	0.049 (2)	−0.0029 (16)	0.0203 (18)	−0.0093 (17)
C19	0.036 (2)	0.034 (2)	0.064 (3)	−0.0003 (18)	0.028 (2)	−0.010 (2)
C20	0.043 (2)	0.044 (2)	0.044 (2)	0.015 (2)	0.002 (2)	−0.001 (2)
C21	0.0231 (17)	0.039 (2)	0.0211 (16)	−0.0025 (15)	0.0046 (14)	−0.0005 (15)
C22	0.051 (3)	0.059 (3)	0.028 (2)	0.004 (2)	0.0018 (19)	−0.009 (2)
C23	0.059 (3)	0.044 (3)	0.038 (2)	0.005 (2)	0.001 (2)	0.010 (2)
C24	0.027 (2)	0.162 (7)	0.038 (3)	−0.004 (3)	0.010 (2)	0.019 (3)
C25	0.0274 (17)	0.0199 (16)	0.0222 (16)	−0.0024 (14)	0.0018 (14)	0.0008 (13)
C26	0.0226 (17)	0.0175 (16)	0.045 (2)	0.0046 (14)	0.0038 (15)	−0.0010 (15)
C27	0.0235 (17)	0.0225 (17)	0.039 (2)	−0.0037 (14)	0.0011 (15)	0.0005 (15)
C28	0.0329 (19)	0.0243 (17)	0.0214 (16)	−0.0046 (15)	0.0075 (14)	−0.0025 (14)
C29	0.0288 (18)	0.0229 (16)	0.0302 (18)	−0.0030 (14)	0.0152 (15)	−0.0069 (14)
C30	0.036 (2)	0.0173 (16)	0.0264 (17)	0.0019 (15)	0.0005 (15)	−0.0006 (14)
C31	0.039 (2)	0.0192 (16)	0.0246 (17)	0.0031 (15)	0.0102 (15)	−0.0017 (13)
C32	0.039 (2)	0.0183 (16)	0.0276 (18)	0.0043 (15)	0.0140 (16)	−0.0003 (14)
C33	0.0363 (19)	0.0208 (16)	0.0285 (18)	0.0054 (15)	0.0180 (15)	0.0046 (14)
C34	0.038 (2)	0.0200 (16)	0.0260 (17)	0.0087 (15)	0.0177 (15)	0.0039 (13)
Cd1	0.02170 (12)	0.01716 (12)	0.02166 (12)	0.00228 (9)	0.00958 (9)	0.00049 (9)

N1	0.0194 (14)	0.0202 (14)	0.0247 (14)	−0.0017 (11)	0.0089 (12)	−0.0020 (11)
N2	0.0200 (14)	0.0194 (13)	0.0246 (14)	0.0005 (11)	0.0063 (11)	−0.0035 (11)
N3	0.0276 (15)	0.0190 (14)	0.0252 (15)	0.0039 (12)	0.0100 (13)	−0.0007 (12)
N4	0.0334 (16)	0.0186 (13)	0.0227 (14)	0.0048 (12)	0.0135 (12)	0.0015 (11)
O1	0.0206 (11)	0.0215 (11)	0.0177 (10)	0.0013 (9)	0.0073 (9)	0.0000 (9)
O2	0.0145 (10)	0.0322 (13)	0.0203 (11)	−0.0020 (10)	0.0031 (9)	0.0062 (10)
O3	0.0175 (10)	0.0190 (11)	0.0200 (11)	0.0000 (9)	0.0037 (9)	0.0016 (9)
O4	0.0247 (12)	0.0251 (12)	0.0272 (12)	−0.0044 (10)	0.0126 (10)	−0.0042 (10)
O5	0.0266 (12)	0.0215 (11)	0.0246 (11)	0.0026 (10)	0.0096 (10)	−0.0013 (10)
O6	0.0271 (12)	0.0297 (13)	0.0233 (12)	−0.0008 (11)	0.0039 (10)	−0.0023 (10)
S1	0.0214 (4)	0.0263 (4)	0.0177 (4)	0.0004 (3)	0.0057 (3)	−0.0009 (3)
S2	0.0342 (5)	0.0212 (4)	0.0345 (5)	0.0011 (4)	0.0223 (4)	0.0012 (3)
Si1	0.0150 (4)	0.0184 (4)	0.0168 (4)	−0.0005 (3)	0.0032 (3)	0.0011 (3)
Si2	0.0192 (4)	0.0221 (4)	0.0194 (4)	−0.0011 (4)	0.0076 (3)	−0.0011 (3)

Geometric parameters (Å, º)

C1—O1	1.448 (4)	C20—H20C	0.98
C1—C3	1.516 (5)	C21—O6	1.436 (4)
C1—C2	1.522 (5)	C21—C24	1.497 (6)
C1—C4	1.525 (5)	C21—C22	1.512 (6)
C2—H2A	0.98	C21—C23	1.515 (6)
C2—H2B	0.98	C22—H22A	0.98
C2—H2C	0.98	C22—H22B	0.98
C3—H3C	0.98	C22—H22C	0.98
C3—H3D	0.98	C23—H23A	0.98
C3—H3E	0.98	C23—H23B	0.98
C4—H4A	0.98	C23—H23C	0.98
C4—H4B	0.98	C24—H24A	0.98
C4—H4C	0.98	C24—H24B	0.98
C5—O2	1.441 (4)	C24—H24C	0.98
C5—C8	1.510 (5)	C25—N1	1.484 (4)
C5—C7	1.515 (6)	C25—C26	1.514 (5)
C5—C6	1.521 (5)	C25—H25A	0.99
C6—H6A	0.98	C25—H25B	0.99
C6—H6B	0.98	C26—C27	1.531 (5)
C6—H6C	0.98	C26—H26A	0.99
C7—H7A	0.98	C26—H26B	0.99
C7—H7B	0.98	C27—N2	1.465 (4)
C7—H7C	0.98	C27—H27A	0.99
C8—H8A	0.98	C27—H27B	0.99
C8—H8B	0.98	C28—N2	1.462 (4)
C8—H8C	0.98	C28—C29^{i}	1.512 (5)
C9—O3	1.456 (4)	C28—H28A	0.99
C9—C12	1.507 (5)	C28—H28B	0.99
C9—C11	1.519 (5)	C29—N2	1.470 (4)
C9—C10	1.520 (5)	C29—H29A	0.99
C10—H10A	0.98	C29—H29B	0.99

C10—H10B	0.98	C30—N3	1.488 (4)
C10—H10C	0.98	C30—C31	1.537 (5)
C11—H11A	0.98	C30—H30A	0.99
C11—H11B	0.98	C30—H30B	0.99
C11—H11C	0.98	C31—C32	1.535 (5)
C12—H12A	0.98	C31—H31A	0.99
C12—H12B	0.98	C31—H31B	0.99
C12—H12C	0.98	C32—N4	1.474 (5)
C13—O4	1.440 (4)	C32—H32A	0.99
C13—C15	1.507 (5)	C32—H32B	0.99
C13—C14	1.529 (5)	C33—N4	1.469 (4)
C13—C16	1.529 (5)	C33—C34^{ii}	1.514 (5)
C14—H14A	0.98	C33—H33A	0.99
C14—H14B	0.98	C33—H33B	0.99
C14—H14C	0.98	C34—N4	1.473 (4)
C15—H15A	0.98	C34—H34A	0.99
C15—H15B	0.98	C34—H34B	0.99
C15—H15C	0.98	Cd1—N3	2.301 (3)
C16—H16A	0.98	Cd1—N1	2.301 (3)
C16—H16B	0.98	Cd1—S2	2.4597 (10)
C16—H16C	0.98	Cd1—S1	2.4675 (12)
C17—O5	1.451 (4)	N1—H1A	0.90 (4)
C17—C18	1.515 (5)	N1—H1B	0.85 (4)
C17—C20	1.524 (5)	N3—H3A	0.96 (4)
C17—C19	1.528 (5)	N3—H3B	0.90 (5)
C18—H18A	0.98	O1—Si1	1.630 (2)
C18—H18B	0.98	O2—Si1	1.627 (2)
C18—H18C	0.98	O3—Si1	1.639 (2)
C19—H19A	0.98	O4—Si2	1.625 (2)
C19—H19B	0.98	O5—Si2	1.647 (2)
C19—H19C	0.98	O6—Si2	1.628 (2)
C20—H20A	0.98	S1—Si1	2.0805 (13)
C20—H20B	0.98	S2—Si2	2.0773 (13)

O1—C1—C3	110.8 (3)	C24—C21—C23	111.6 (4)
O1—C1—C2	110.0 (3)	C22—C21—C23	109.1 (4)
C3—C1—C2	110.6 (3)	C21—C22—H22A	109.5
O1—C1—C4	105.1 (3)	C21—C22—H22B	109.5
C3—C1—C4	110.2 (3)	H22A—C22—H22B	109.5
C2—C1—C4	110.0 (3)	C21—C22—H22C	109.5
C1—C2—H2A	109.5	H22A—C22—H22C	109.5
C1—C2—H2B	109.5	H22B—C22—H22C	109.5
H2A—C2—H2B	109.5	C21—C23—H23A	109.5
C1—C2—H2C	109.5	C21—C23—H23B	109.5
H2A—C2—H2C	109.5	H23A—C23—H23B	109.5
H2B—C2—H2C	109.5	C21—C23—H23C	109.5
C1—C3—H3C	109.5	H23A—C23—H23C	109.5
C1—C3—H3D	109.5	H23B—C23—H23C	109.5

H3C—C3—H3D	109.5	C21—C24—H24A	109.5
C1—C3—H3E	109.5	C21—C24—H24B	109.5
H3C—C3—H3E	109.5	H24A—C24—H24B	109.5
H3D—C3—H3E	109.5	C21—C24—H24C	109.5
C1—C4—H4A	109.5	H24A—C24—H24C	109.5
C1—C4—H4B	109.5	H24B—C24—H24C	109.5
H4A—C4—H4B	109.5	N1—C25—C26	111.9 (3)
C1—C4—H4C	109.5	N1—C25—H25A	109.2
H4A—C4—H4C	109.5	C26—C25—H25A	109.2
H4B—C4—H4C	109.5	N1—C25—H25B	109.2
O2—C5—C8	105.7 (3)	C26—C25—H25B	109.2
O2—C5—C7	109.2 (3)	H25A—C25—H25B	107.9
C8—C5—C7	110.2 (4)	C25—C26—C27	113.9 (3)
O2—C5—C6	110.3 (3)	C25—C26—H26A	108.8
C8—C5—C6	110.2 (3)	C27—C26—H26A	108.8
C7—C5—C6	111.2 (3)	C25—C26—H26B	108.8
C5—C6—H6A	109.5	C27—C26—H26B	108.8
C5—C6—H6B	109.5	H26A—C26—H26B	107.7
H6A—C6—H6B	109.5	N2—C27—C26	113.4 (3)
C5—C6—H6C	109.5	N2—C27—H27A	108.9
H6A—C6—H6C	109.5	C26—C27—H27A	108.9
H6B—C6—H6C	109.5	N2—C27—H27B	108.9
C5—C7—H7A	109.5	C26—C27—H27B	108.9
C5—C7—H7B	109.5	H27A—C27—H27B	107.7
H7A—C7—H7B	109.5	N2—C28—C29^{i}	110.4 (3)
C5—C7—H7C	109.5	N2—C28—H28A	109.6
H7A—C7—H7C	109.5	C29^{i}—C28—H28A	109.6
H7B—C7—H7C	109.5	N2—C28—H28B	109.6
C5—C8—H8A	109.5	C29^{i}—C28—H28B	109.6
C5—C8—H8B	109.5	H28A—C28—H28B	108.1
H8A—C8—H8B	109.5	N2—C29—C28^{i}	110.9 (3)
C5—C8—H8C	109.5	N2—C29—H29A	109.5
H8A—C8—H8C	109.5	C28^{i}—C29—H29A	109.5
H8B—C8—H8C	109.5	N2—C29—H29B	109.5
O3—C9—C12	110.6 (3)	C28^{i}—C29—H29B	109.5
O3—C9—C11	109.9 (3)	H29A—C29—H29B	108.1
C12—C9—C11	110.8 (3)	N3—C30—C31	114.0 (3)
O3—C9—C10	104.5 (3)	N3—C30—H30A	108.7
C12—C9—C10	111.1 (3)	C31—C30—H30A	108.7
C11—C9—C10	109.9 (3)	N3—C30—H30B	108.7
C9—C10—H10A	109.5	C31—C30—H30B	108.7
C9—C10—H10B	109.5	H30A—C30—H30B	107.6
H10A—C10—H10B	109.5	C32—C31—C30	114.0 (3)
C9—C10—H10C	109.5	C32—C31—H31A	108.8
H10A—C10—H10C	109.5	C30—C31—H31A	108.8
H10B—C10—H10C	109.5	C32—C31—H31B	108.8
C9—C11—H11A	109.5	C30—C31—H31B	108.8
C9—C11—H11B	109.5	H31A—C31—H31B	107.6

H11A—C11—H11B	109.5	N4—C32—C31	114.9 (3)
C9—C11—H11C	109.5	N4—C32—H32A	108.5
H11A—C11—H11C	109.5	C31—C32—H32A	108.5
H11B—C11—H11C	109.5	N4—C32—H32B	108.5
C9—C12—H12A	109.5	C31—C32—H32B	108.5
C9—C12—H12B	109.5	H32A—C32—H32B	107.5
H12A—C12—H12B	109.5	N4—C33—C34^{ii}	111.5 (3)
C9—C12—H12C	109.5	N4—C33—H33A	109.3
H12A—C12—H12C	109.5	C34^{ii}—C33—H33A	109.3
H12B—C12—H12C	109.5	N4—C33—H33B	109.3
O4—C13—C15	109.9 (3)	C34^{ii}—C33—H33B	109.3
O4—C13—C14	110.2 (3)	H33A—C33—H33B	108
C15—C13—C14	111.0 (3)	N4—C34—C33^{ii}	111.3 (3)
O4—C13—C16	105.5 (3)	N4—C34—H34A	109.4
C15—C13—C16	110.1 (3)	C33^{ii}—C34—H34A	109.4
C14—C13—C16	110.0 (3)	N4—C34—H34B	109.4
C13—C14—H14A	109.5	C33^{ii}—C34—H34B	109.4
C13—C14—H14B	109.5	H34A—C34—H34B	108
H14A—C14—H14B	109.5	N3—Cd1—N1	99.26 (10)
C13—C14—H14C	109.5	N3—Cd1—S2	109.68 (8)
H14A—C14—H14C	109.5	N1—Cd1—S2	111.36 (8)
H14B—C14—H14C	109.5	N3—Cd1—S1	107.26 (8)
C13—C15—H15A	109.5	N1—Cd1—S1	106.89 (8)
C13—C15—H15B	109.5	S2—Cd1—S1	120.28 (3)
H15A—C15—H15B	109.5	C25—N1—Cd1	117.7 (2)
C13—C15—H15C	109.5	C25—N1—H1A	105 (2)
H15A—C15—H15C	109.5	Cd1—N1—H1A	115 (2)
H15B—C15—H15C	109.5	C25—N1—H1B	111 (3)
C13—C16—H16A	109.5	Cd1—N1—H1B	103 (3)
C13—C16—H16B	109.5	H1A—N1—H1B	105 (4)
H16A—C16—H16B	109.5	C28—N2—C27	110.9 (3)
C13—C16—H16C	109.5	C28—N2—C29	108.4 (3)
H16A—C16—H16C	109.5	C27—N2—C29	111.0 (3)
H16B—C16—H16C	109.5	C30—N3—Cd1	115.7 (2)
O5—C17—C18	109.3 (3)	C30—N3—H3A	111 (2)
O5—C17—C20	105.0 (3)	Cd1—N3—H3A	110 (2)
C18—C17—C20	110.5 (3)	C30—N3—H3B	112 (3)
O5—C17—C19	112.1 (3)	Cd1—N3—H3B	105 (3)
C18—C17—C19	109.1 (3)	H3A—N3—H3B	102 (4)
C20—C17—C19	110.9 (3)	C33—N4—C34	107.7 (3)
C17—C18—H18A	109.5	C33—N4—C32	109.8 (3)
C17—C18—H18B	109.5	C34—N4—C32	111.5 (3)
H18A—C18—H18B	109.5	C1—O1—Si1	132.1 (2)
C17—C18—H18C	109.5	C5—O2—Si1	134.2 (2)
H18A—C18—H18C	109.5	C9—O3—Si1	132.0 (2)
H18B—C18—H18C	109.5	C13—O4—Si2	134.4 (2)
C17—C19—H19A	109.5	C17—O5—Si2	129.2 (2)
C17—C19—H19B	109.5	C21—O6—Si2	133.8 (2)

H19A—C19—H19B	109.5	Si1—S1—Cd1	104.26 (5)
C17—C19—H19C	109.5	Si2—S2—Cd1	110.61 (5)
H19A—C19—H19C	109.5	O2—Si1—O1	112.37 (13)
H19B—C19—H19C	109.5	O2—Si1—O3	105.53 (12)
C17—C20—H20A	109.5	O1—Si1—O3	102.90 (12)
C17—C20—H20B	109.5	O2—Si1—S1	110.91 (10)
H20A—C20—H20B	109.5	O1—Si1—S1	108.96 (9)
C17—C20—H20C	109.5	O3—Si1—S1	115.98 (9)
H20A—C20—H20C	109.5	O4—Si2—O6	105.24 (13)
H20B—C20—H20C	109.5	O4—Si2—O5	111.65 (13)
O6—C21—C24	107.9 (3)	O6—Si2—O5	102.77 (13)
O6—C21—C22	105.6 (3)	O4—Si2—S2	110.06 (10)
C24—C21—C22	111.3 (4)	O6—Si2—S2	115.55 (11)
O6—C21—C23	111.1 (3)	O5—Si2—S2	111.29 (10)

N1—C25—C26—C27	−73.5 (4)	C15—C13—O4—Si2	80.1 (4)
C25—C26—C27—N2	64.1 (4)	C14—C13—O4—Si2	−42.6 (4)
N3—C30—C31—C32	−66.8 (4)	C16—C13—O4—Si2	−161.3 (3)
C30—C31—C32—N4	64.0 (4)	C18—C17—O5—Si2	84.9 (4)
C26—C25—N1—Cd1	−77.8 (3)	C20—C17—O5—Si2	−156.6 (3)
C29^{i}—C28—N2—C27	179.5 (3)	C19—C17—O5—Si2	−36.2 (4)
C29^{i}—C28—N2—C29	−58.4 (4)	C24—C21—O6—Si2	87.7 (5)
C26—C27—N2—C28	−161.7 (3)	C22—C21—O6—Si2	−153.3 (3)
C26—C27—N2—C29	77.7 (4)	C23—C21—O6—Si2	−35.1 (5)
C28^{i}—C29—N2—C28	58.7 (4)	C5—O2—Si1—O1	−87.0 (3)
C28^{i}—C29—N2—C27	−179.3 (3)	C5—O2—Si1—O3	161.6 (3)
C31—C30—N3—Cd1	167.7 (2)	C5—O2—Si1—S1	35.2 (3)
C34^{ii}—C33—N4—C34	−57.6 (4)	C1—O1—Si1—O2	−60.1 (3)
C34^{ii}—C33—N4—C32	−179.2 (3)	C1—O1—Si1—O3	52.9 (3)
C33^{ii}—C34—N4—C33	57.5 (4)	C1—O1—Si1—S1	176.5 (2)
C33^{ii}—C34—N4—C32	177.9 (3)	C9—O3—Si1—O2	−44.0 (3)
C31—C32—N4—C33	−171.8 (3)	C9—O3—Si1—O1	−162.0 (3)
C31—C32—N4—C34	69.0 (4)	C9—O3—Si1—S1	79.2 (3)
C3—C1—O1—Si1	43.1 (4)	C13—O4—Si2—O6	−172.1 (3)
C2—C1—O1—Si1	−79.6 (4)	C13—O4—Si2—O5	77.1 (3)
C4—C1—O1—Si1	162.1 (2)	C13—O4—Si2—S2	−47.0 (3)
C8—C5—O2—Si1	160.0 (3)	C21—O6—Si2—O4	72.9 (3)
C7—C5—O2—Si1	−81.5 (4)	C21—O6—Si2—O5	−170.2 (3)
C6—C5—O2—Si1	41.0 (5)	C21—O6—Si2—S2	−48.8 (3)
C12—C9—O3—Si1	−50.6 (4)	C17—O5—Si2—O4	61.8 (3)
C11—C9—O3—Si1	72.0 (4)	C17—O5—Si2—O6	−50.5 (3)
C10—C9—O3—Si1	−170.2 (2)	C17—O5—Si2—S2	−174.8 (2)

Symmetry codes: (i) −*x*+1, −*y*, −*z*+1; (ii) −*x*+1, −*y*+1, −*z*+1.

Hydrogen-bond geometry (Å, º)

D—H···*A*	*D*—H	H···*A*	*D*···*A*	*D*—H···*A*
N1—H1*A*···N2	0.90 (4)	2.24 (4)	2.977 (4)	139 (3)

N3—H3*A*···N4	0.96 (4)	2.23 (4)	2.996 (4)	136 (3)
N3—H3*B*···O5	0.90 (5)	2.42 (5)	3.256 (4)	154 (4)
N1—H1*B*···O3	0.85 (4)	2.39 (4)	3.200 (4)	160 (3)
N1—H1*A*···N2	0.90 (4)	2.24 (4)	2.977 (4)	139 (3)
N3—H3*A*···N4	0.96 (4)	2.23 (4)	2.996 (4)	136 (3)
N3—H3*B*···O5	0.90 (5)	2.42 (5)	3.256 (4)	154 (4)
N1—H1*B*···O3	0.85 (4)	2.39 (4)	3.200 (4)	160 (3)

μ-1,4-Bis(3-aminopropyl)piperazine-$\kappa^4N^1,N^{1'}$:$N^4,N^{4'}$-bis[bis(tri-*tert*-butoxysilanethiolato-κS)cadmium(II)] (dkz1)

Crystal data

$[Cd_2(C_{12}H_{27}O_3SSi)_4(C_{10}H_{24}N_4)]$
M_r = 1543.07
Monoclinic, $P2_1/n$
Hall symbol: -P 2yn
a = 9.6433 (2) Å
b = 29.0546 (4) Å
c = 14.5665 (2) Å
β = 91.466 (1)°
V = 4079.94 (12) Å^3
Z = 2
$F(000)$ = 1640
D_x = 1.256 Mg m^{-3}
Mo $K\alpha$ radiation, λ = 0.71073 Å
Cell parameters from 67652 reflections
θ = 2.2–29.6°
μ = 0.73 mm^{-1}
T = 120 K
Prism, colorless
0.44 × 0.26 × 0.14 mm

Data collection

Stoe IPDS 2T diffractometer
Radiation source: GeniX Mo, 0.05 x 0.05 mm2 microfocus
Parabolic x-ray mirror monochromator
Detector resolution: 6.67 pixels mm^{-1}
rotation method, ω scans
Absorption correction: multi-scan [LANA (Koziskova *et al.*, 2016) in X-AREA (Stoe & Cie, 2016)]
T_{min} = 0.409, T_{max} = 1.000
39464 measured reflections
8337 independent reflections
7133 reflections with $I > 2\sigma(I)$
R_{int} = 0.028
θ_{max} = 26.4°, θ_{min} = 2.2°
h = −12→11
k = −36→36
l = −18→18

Refinement

Refinement on F^2
Least-squares matrix: full
$R[F^2 > 2\sigma(F^2)]$ = 0.044
$wR(F^2)$ = 0.123
S = 1.04
8337 reflections
424 parameters
0 restraints
0 constraints
Hydrogen site location: mixed
H atoms treated by a mixture of independent and constrained refinement
$w = 1/[\sigma^2(F_o^2) + (0.0649P)^2 + 6.3741P]$ where $P = (F_o^2 + 2F_c^2)/3$
$(\Delta/\sigma)_{max}$ = 0.002
$\Delta\rho_{max}$ = 1.52 e Å^{-3}
$\Delta\rho_{min}$ = −0.70 e Å^{-3}

Special details

Geometry. All esds (except the esd in the dihedral angle between two l.s. planes) are estimated using the full covariance matrix. The cell esds are taken into account individually in the estimation of esds in distances, angles and torsion angles; correlations between esds in cell parameters are only used when they are defined by crystal symmetry. An approximate (isotropic) treatment of cell esds is used for estimating esds involving l.s. planes.

Refinement. Single-crystal X-ray diffraction data of compounds **1** and **2** were collected at 120 (2) K with a Stoe IPDS-2T diffractometer equipped with a graphite-monochromated Mo *Kα* radiation source. Crystals were cooled using a Cryostream 800 open-flow nitrogen cryostat (Oxford Cryosystems). Data collection and image processing was performed with X-AREA 1.75 (Stoe & Cie, 2016). Intensity data were scaled with LANA (part of X-AREA) in order to minimize differences in intensities of symmetry-equivalent reflections (a multi-scan method). The structures of **1** and **2** were solved using intrinsic phasing procedure implemented in SHELXT and all non-hydrogen atoms were refined with anisotropic displacement parameters by full-matrix least squares procedure based on F^2 using the SHELX–2014 program package (Sheldrick, 2014; Sheldrick, 2015). The OLEX2 (Dolomanov *et al.*, 2009) and Wingx (Farrugia, 2012) program suites were used to prepare the final version of CIF files. Mercury (Macrae *et al.*, 2020) was used to prepare the figures.

Fractional atomic coordinates and isotropic or equivalent isotropic displacement parameters (Å²)

	x	*y*	*z*	U_{iso}*/U_{eq}	Occ. (<1)
C1	0.5588 (5)	0.5996 (2)	0.8558 (4)	0.0749 (14)	
C2	0.5340 (5)	0.63359 (19)	0.7809 (5)	0.095 (2)	
H2A	0.609754	0.65608	0.781186	0.143*	
H2B	0.445922	0.649503	0.790336	0.143*	
H2C	0.530017	0.617576	0.721636	0.143*	
C3	0.4417 (5)	0.5648 (2)	0.8601 (5)	0.097 (2)	
H3A	0.430415	0.549423	0.800432	0.146*	
H3B	0.355367	0.580585	0.874924	0.146*	
H3C	0.463855	0.541856	0.907546	0.146*	
C4	0.5806 (7)	0.6229 (3)	0.9496 (5)	0.137 (4)	
H4A	0.601812	0.599425	0.99622	0.206*	
H4B	0.495935	0.639338	0.965748	0.206*	
H4C	0.65784	0.644674	0.946676	0.206*	
C5	0.8052 (5)	0.47142 (15)	0.8720 (3)	0.0618 (11)	
C6	0.7957 (6)	0.4939 (2)	0.9672 (3)	0.0762 (15)	
H6A	0.884169	0.508724	0.983452	0.114*	
H6B	0.775124	0.470267	1.012881	0.114*	
H6C	0.721587	0.516991	0.965833	0.114*	
C7	0.6661 (6)	0.4510 (2)	0.8429 (4)	0.0844 (17)	
H7A	0.594647	0.474988	0.844409	0.127*	
H7B	0.642219	0.426136	0.885017	0.127*	
H7C	0.671514	0.438794	0.780362	0.127*	
C8	0.9188 (7)	0.43555 (17)	0.8713 (5)	0.0875 (18)	
H8A	0.921653	0.421322	0.810427	0.131*	
H8B	0.900089	0.411897	0.91736	0.131*	
H8C	1.008229	0.450199	0.88585	0.131*	
C9	0.9872 (4)	0.61315 (11)	0.7731 (2)	0.0428 (8)	
C10	1.0344 (4)	0.59065 (14)	0.8613 (3)	0.0528 (9)	
H10A	0.956481	0.588852	0.903011	0.079*	
H10B	1.109331	0.608851	0.889907	0.079*	
H10C	1.068212	0.559557	0.84844	0.079*	
C11	1.1119 (5)	0.61852 (16)	0.7099 (3)	0.0619 (11)	
H11A	1.157037	0.588581	0.702246	0.093*	
H11B	1.178369	0.640354	0.73735	0.093*	
H11C	1.079681	0.63002	0.649773	0.093*	
C12	0.9228 (5)	0.65858 (15)	0.7876 (4)	0.0738 (14)	

H12A	0.882495	0.66984	0.729404	0.111*
H12B	0.993513	0.680319	0.810246	0.111*
H12C	0.849816	0.655759	0.832838	0.111*
C13	0.4108 (4)	0.67627 (13)	0.4306 (3)	0.0457 (8)
C14	0.3193 (5)	0.65446 (19)	0.5000 (4)	0.0782 (15)
H14A	0.325732	0.620891	0.495232	0.117*
H14B	0.22301	0.664081	0.488269	0.117*
H14C	0.349184	0.664165	0.561803	0.117*
C15	0.3950 (5)	0.72749 (16)	0.4309 (5)	0.0850 (18)
H15A	0.420542	0.739487	0.491886	0.127*
H15B	0.298334	0.735542	0.415877	0.127*
H15C	0.455629	0.740988	0.38514	0.127*
C16	0.3733 (5)	0.6568 (2)	0.3361 (4)	0.092 (2)
H16A	0.436021	0.669522	0.290678	0.138*
H16B	0.277481	0.665102	0.319355	0.138*
H16C	0.382362	0.623194	0.337415	0.138*
C17	0.7558 (5)	0.76129 (14)	0.5443 (3)	0.0592 (11)
C18	0.6874 (6)	0.73649 (18)	0.6259 (3)	0.0728 (13)
H18A	0.586574	0.735938	0.615913	0.109*
H18B	0.710126	0.752992	0.683023	0.109*
H18C	0.722449	0.704884	0.630356	0.109*
C19	0.9114 (5)	0.76228 (18)	0.5556 (5)	0.0854 (18)
H19A	0.946356	0.730801	0.563261	0.128*
H19B	0.937499	0.78054	0.609939	0.128*
H19C	0.951673	0.776141	0.501068	0.128*
C20	0.6968 (6)	0.81000 (16)	0.5331 (5)	0.0841 (17)
H20A	0.7371	0.824684	0.479431	0.126*
H20B	0.719876	0.828109	0.588196	0.126*
H20C	0.595816	0.808352	0.524643	0.126*
C21	0.7964 (5)	0.70335 (16)	0.2538 (3)	0.0589 (11)
C22	0.7513 (6)	0.75199 (17)	0.2354 (4)	0.0760 (14)
H22A	0.655537	0.752091	0.211282	0.114*
H22B	0.812191	0.765916	0.190241	0.114*
H22C	0.756867	0.769709	0.292611	0.114*
C23	0.7778 (7)	0.6750 (2)	0.1673 (4)	0.0903 (18)
H23A	0.814866	0.64399	0.17792	0.135*
H23B	0.827675	0.68964	0.117249	0.135*
H23C	0.678949	0.673005	0.150522	0.135*
C24	0.9449 (5)	0.7001 (3)	0.2888 (5)	0.110 (3)
H24A	0.957238	0.719357	0.343654	0.165*
H24B	1.007119	0.710839	0.241098	0.165*
H24C	0.966823	0.668064	0.304286	0.165*
C25	0.6447 (5)	0.56335 (16)	0.3111 (3)	0.0597 (11)
H25A	0.68287	0.594731	0.30369	0.072*
H25B	0.567501	0.559657	0.265539	0.072*
C26	0.8977 (5)	0.54003 (16)	0.3355 (3)	0.0575 (10)
H26A	0.967787	0.523448	0.299611	0.069*
H26B	0.917402	0.57335	0.330286	0.069*

C27	0.7513 (6)	0.53043 (17)	0.2910 (3)	0.0692 (13)	
H27A	0.760771	0.529008	0.22354	0.083*	
H27B	0.720132	0.499725	0.311532	0.083*	
C28	0.9024 (4)	0.47707 (14)	0.4433 (3)	0.0513 (9)	
H28A	0.96518	0.461824	0.399961	0.062*	
H28B	0.806228	0.467714	0.426877	0.062*	
C29	1.0624 (4)	0.53866 (13)	0.4609 (3)	0.0472 (8)	
H29A	1.126508	0.524071	0.417599	0.057*	
H29B	1.074611	0.572426	0.456899	0.057*	
Cd1	0.75028 (2)	0.57009 (2)	0.52053 (2)	0.03435 (9)	
O1	0.6846 (3)	0.57472 (10)	0.84279 (18)	0.0516 (7)	
O2	0.8463 (3)	0.50641 (8)	0.80641 (18)	0.0471 (6)	
O3	0.8888 (3)	0.58334 (8)	0.72319 (16)	0.0423 (5)	
O4	0.5517 (2)	0.66226 (8)	0.45481 (17)	0.0399 (5)	
O5	0.7181 (3)	0.73814 (8)	0.45944 (19)	0.0468 (6)	
O6	0.7036 (3)	0.68365 (9)	0.31954 (17)	0.0483 (6)	
N1	0.5903 (3)	0.55928 (12)	0.4017 (2)	0.0453 (7)	
N2	0.9149 (3)	0.52636 (11)	0.4339 (2)	0.0495 (7)	
S1	0.6456 (7)	0.53026 (17)	0.6479 (3)	0.0345 (8)	0.79 (3)
S1A	0.607 (3)	0.5374 (8)	0.6507 (12)	0.046 (3)	0.21 (3)
S2	0.8577 (3)	0.64623 (17)	0.4982 (4)	0.0356 (6)	0.79 (3)
S2A	0.8612 (14)	0.6350 (10)	0.468 (3)	0.049 (6)	0.21 (3)
Si1	0.76506 (10)	0.55055 (3)	0.76074 (6)	0.0356 (2)	
Si2	0.70303 (9)	0.68408 (3)	0.43116 (6)	0.0353 (2)	
H1A	0.535 (5)	0.5363 (17)	0.406 (3)	0.059 (13)*	
H1B	0.540 (5)	0.5817 (16)	0.415 (3)	0.055 (13)*	

Atomic displacement parameters (Å²)

	U^{11}	U^{22}	U^{33}	U^{12}	U^{13}	U^{23}
C1	0.051 (2)	0.095 (4)	0.079 (3)	0.011 (2)	0.003 (2)	−0.033 (3)
C2	0.058 (3)	0.066 (3)	0.162 (6)	0.023 (2)	−0.010 (3)	−0.021 (4)
C3	0.046 (3)	0.143 (6)	0.103 (5)	0.003 (3)	0.015 (3)	−0.007 (4)
C4	0.087 (4)	0.198 (8)	0.127 (6)	0.038 (5)	0.009 (4)	−0.107 (6)
C5	0.060 (2)	0.051 (2)	0.074 (3)	−0.0213 (19)	−0.012 (2)	0.020 (2)
C6	0.077 (3)	0.093 (4)	0.057 (3)	−0.024 (3)	−0.012 (2)	0.027 (3)
C7	0.083 (4)	0.083 (4)	0.086 (4)	−0.044 (3)	−0.014 (3)	0.024 (3)
C8	0.107 (5)	0.047 (3)	0.107 (5)	0.000 (3)	−0.012 (4)	0.022 (3)
C9	0.051 (2)	0.0323 (16)	0.0448 (18)	−0.0139 (15)	−0.0060 (15)	−0.0050 (14)
C10	0.052 (2)	0.055 (2)	0.050 (2)	−0.0161 (18)	−0.0107 (17)	0.0024 (18)
C11	0.068 (3)	0.064 (3)	0.054 (2)	−0.032 (2)	0.007 (2)	−0.011 (2)
C12	0.073 (3)	0.040 (2)	0.108 (4)	0.001 (2)	−0.021 (3)	−0.019 (2)
C13	0.0313 (17)	0.0438 (19)	0.062 (2)	0.0045 (14)	0.0025 (15)	−0.0015 (17)
C14	0.045 (2)	0.080 (3)	0.109 (4)	−0.006 (2)	0.013 (3)	0.021 (3)
C15	0.042 (2)	0.048 (2)	0.164 (6)	0.0092 (19)	−0.012 (3)	0.011 (3)
C16	0.058 (3)	0.136 (5)	0.081 (4)	0.036 (3)	−0.026 (3)	−0.024 (4)
C17	0.062 (3)	0.039 (2)	0.075 (3)	0.0043 (18)	−0.021 (2)	−0.0077 (19)
C18	0.087 (4)	0.074 (3)	0.058 (3)	0.019 (3)	−0.006 (2)	−0.010 (2)

C19	0.061 (3)	0.057 (3)	0.136 (5)	−0.007 (2)	−0.036 (3)	0.001 (3)
C20	0.082 (3)	0.041 (2)	0.127 (5)	0.007 (2)	−0.036 (3)	−0.013 (3)
C21	0.065 (3)	0.061 (3)	0.051 (2)	0.012 (2)	0.0159 (19)	0.0226 (19)
C22	0.086 (3)	0.063 (3)	0.079 (3)	0.007 (3)	0.011 (3)	0.029 (3)
C23	0.121 (5)	0.086 (4)	0.065 (3)	0.030 (4)	0.032 (3)	0.013 (3)
C24	0.050 (3)	0.160 (6)	0.121 (5)	0.013 (3)	0.031 (3)	0.079 (5)
C25	0.070 (3)	0.063 (3)	0.045 (2)	−0.010 (2)	−0.015 (2)	−0.0003 (19)
C26	0.071 (3)	0.055 (2)	0.047 (2)	0.007 (2)	0.0044 (19)	−0.0032 (18)
C27	0.095 (4)	0.066 (3)	0.045 (2)	0.007 (3)	−0.020 (2)	−0.009 (2)
C28	0.053 (2)	0.049 (2)	0.052 (2)	−0.0096 (17)	−0.0019 (17)	−0.0039 (17)
C29	0.052 (2)	0.0387 (18)	0.051 (2)	−0.0152 (16)	0.0028 (16)	−0.0003 (15)
Cd1	0.03965 (15)	0.02768 (13)	0.03571 (14)	0.00312 (9)	0.00060 (9)	−0.00117 (9)
O1	0.0463 (14)	0.0671 (18)	0.0416 (14)	0.0015 (12)	0.0030 (11)	−0.0168 (12)
O2	0.0465 (14)	0.0386 (13)	0.0558 (15)	−0.0086 (11)	−0.0031 (12)	0.0080 (11)
O3	0.0510 (14)	0.0396 (12)	0.0361 (12)	−0.0166 (11)	−0.0060 (10)	−0.0016 (10)
O4	0.0325 (12)	0.0377 (12)	0.0493 (13)	−0.0004 (9)	−0.0022 (10)	0.0046 (10)
O5	0.0442 (14)	0.0365 (13)	0.0595 (15)	0.0013 (10)	−0.0041 (12)	0.0045 (11)
O6	0.0452 (14)	0.0556 (15)	0.0443 (14)	0.0114 (12)	0.0062 (11)	0.0106 (12)
N1	0.0406 (16)	0.0336 (15)	0.061 (2)	−0.0015 (14)	−0.0073 (14)	−0.0045 (14)
N2	0.0546 (19)	0.0474 (18)	0.0461 (17)	0.0029 (14)	−0.0058 (14)	−0.0028 (14)
S1	0.0320 (17)	0.0389 (12)	0.0326 (8)	−0.0092 (10)	−0.0008 (10)	−0.0026 (7)
S1A	0.038 (7)	0.056 (6)	0.043 (3)	−0.008 (5)	−0.002 (4)	−0.012 (4)
S2	0.0366 (7)	0.0252 (10)	0.0446 (14)	0.0020 (6)	−0.0061 (7)	0.0023 (9)
S2A	0.033 (3)	0.036 (7)	0.077 (12)	−0.008 (3)	−0.016 (5)	0.021 (8)
Si1	0.0413 (5)	0.0346 (5)	0.0309 (4)	−0.0071 (4)	0.0005 (4)	−0.0009 (3)
Si2	0.0327 (4)	0.0322 (4)	0.0411 (5)	0.0022 (3)	0.0005 (4)	0.0059 (4)

Geometric parameters (Å, º)

C1—O1	1.430 (5)	C18—H18B	0.98
C1—C2	1.486 (9)	C18—H18C	0.98
C1—C3	1.519 (8)	C19—H19A	0.98
C1—C4	1.533 (8)	C19—H19B	0.98
C2—H2A	0.98	C19—H19C	0.98
C2—H2B	0.98	C20—H20A	0.98
C2—H2C	0.98	C20—H20B	0.98
C3—H3A	0.98	C20—H20C	0.98
C3—H3B	0.98	C21—O6	1.445 (5)
C3—H3C	0.98	C21—C22	1.501 (6)
C4—H4A	0.98	C21—C24	1.510 (7)
C4—H4B	0.98	C21—C23	1.513 (7)
C4—H4C	0.98	C22—H22A	0.98
C5—O2	1.457 (5)	C22—H22B	0.98
C5—C8	1.512 (7)	C22—H22C	0.98
C5—C7	1.517 (6)	C23—H23A	0.98
C5—C6	1.538 (7)	C23—H23B	0.98
C6—H6A	0.98	C23—H23C	0.98
C6—H6B	0.98	C24—H24A	0.98

C6—H6C	0.98	C24—H24B	0.98
C7—H7A	0.98	C24—H24C	0.98
C7—H7B	0.98	C25—N1	1.439 (6)
C7—H7C	0.98	C25—C27	1.440 (7)
C8—H8A	0.98	C25—H25A	0.99
C8—H8B	0.98	C25—H25B	0.99
C8—H8C	0.98	C26—N2	1.493 (5)
C9—O3	1.464 (4)	C26—C27	1.563 (7)
C9—C12	1.476 (5)	C26—H26A	0.99
C9—C10	1.502 (5)	C26—H26B	0.99
C9—C11	1.542 (6)	C27—H27A	0.99
C10—H10A	0.98	C27—H27B	0.99
C10—H10B	0.98	C28—N2	1.444 (5)
C10—H10C	0.98	C28—C29^{i}	1.499 (5)
C11—H11A	0.98	C28—H28A	0.99
C11—H11B	0.98	C28—H28B	0.99
C11—H11C	0.98	C29—N2	1.508 (5)
C12—H12A	0.98	C29—H29A	0.99
C12—H12B	0.98	C29—H29B	0.99
C12—H12C	0.98	Cd1—S2A	2.309 (10)
C13—O4	1.453 (4)	Cd1—N1	2.310 (3)
C13—C15	1.496 (6)	Cd1—N2	2.415 (3)
C13—C14	1.499 (6)	Cd1—S1	2.428 (4)
C13—C16	1.523 (6)	Cd1—S2	2.468 (5)
C14—H14A	0.98	Cd1—S1A	2.56 (2)
C14—H14B	0.98	O1—Si1	1.603 (3)
C14—H14C	0.98	O2—Si1	1.635 (3)
C15—H15A	0.98	O3—Si1	1.632 (2)
C15—H15B	0.98	O4—Si2	1.636 (2)
C15—H15C	0.98	O5—Si2	1.629 (3)
C16—H16A	0.98	O6—Si2	1.626 (3)
C16—H16B	0.98	N1—H1A	0.86 (5)
C16—H16C	0.98	N1—H1B	0.84 (5)
C17—O5	1.445 (5)	S1—Si1	2.068 (4)
C17—C19	1.506 (6)	S1A—Si1	2.22 (2)
C17—C20	1.532 (6)	S2—S2A	0.55 (5)
C17—C18	1.551 (7)	S2—Si2	2.077 (3)
C18—H18A	0.98	S2A—Si2	2.146 (18)

O1—C1—C2	111.1 (4)	H20A—C20—H20B	109.5
O1—C1—C3	107.6 (5)	C17—C20—H20C	109.5
C2—C1—C3	111.5 (5)	H20A—C20—H20C	109.5
O1—C1—C4	104.1 (4)	H20B—C20—H20C	109.5
C2—C1—C4	112.2 (6)	O6—C21—C22	108.0 (4)
C3—C1—C4	110.0 (6)	O6—C21—C24	110.5 (3)
C1—C2—H2A	109.5	C22—C21—C24	112.7 (5)
C1—C2—H2B	109.5	O6—C21—C23	105.9 (4)
H2A—C2—H2B	109.5	C22—C21—C23	109.6 (4)

C1—C2—H2C	109.5	C24—C21—C23	109.8 (5)
H2A—C2—H2C	109.5	C21—C22—H22A	109.5
H2B—C2—H2C	109.5	C21—C22—H22B	109.5
C1—C3—H3A	109.5	H22A—C22—H22B	109.5
C1—C3—H3B	109.5	C21—C22—H22C	109.5
H3A—C3—H3B	109.5	H22A—C22—H22C	109.5
C1—C3—H3C	109.5	H22B—C22—H22C	109.5
H3A—C3—H3C	109.5	C21—C23—H23A	109.5
H3B—C3—H3C	109.5	C21—C23—H23B	109.5
C1—C4—H4A	109.5	H23A—C23—H23B	109.5
C1—C4—H4B	109.5	C21—C23—H23C	109.5
H4A—C4—H4B	109.5	H23A—C23—H23C	109.5
C1—C4—H4C	109.5	H23B—C23—H23C	109.5
H4A—C4—H4C	109.5	C21—C24—H24A	109.5
H4B—C4—H4C	109.5	C21—C24—H24B	109.5
O2—C5—C8	105.5 (4)	H24A—C24—H24B	109.5
O2—C5—C7	110.1 (4)	C21—C24—H24C	109.5
C8—C5—C7	111.4 (5)	H24A—C24—H24C	109.5
O2—C5—C6	108.6 (3)	H24B—C24—H24C	109.5
C8—C5—C6	111.0 (4)	N1—C25—C27	114.2 (4)
C7—C5—C6	110.2 (4)	N1—C25—H25A	108.7
C5—C6—H6A	109.5	C27—C25—H25A	108.7
C5—C6—H6B	109.5	N1—C25—H25B	108.7
H6A—C6—H6B	109.5	C27—C25—H25B	108.7
C5—C6—H6C	109.5	H25A—C25—H25B	107.6
H6A—C6—H6C	109.5	N2—C26—C27	115.3 (4)
H6B—C6—H6C	109.5	N2—C26—H26A	108.4
C5—C7—H7A	109.5	C27—C26—H26A	108.4
C5—C7—H7B	109.5	N2—C26—H26B	108.4
H7A—C7—H7B	109.5	C27—C26—H26B	108.4
C5—C7—H7C	109.5	H26A—C26—H26B	107.5
H7A—C7—H7C	109.5	C25—C27—C26	116.1 (4)
H7B—C7—H7C	109.5	C25—C27—H27A	108.3
C5—C8—H8A	109.5	C26—C27—H27A	108.3
C5—C8—H8B	109.5	C25—C27—H27B	108.3
H8A—C8—H8B	109.5	C26—C27—H27B	108.3
C5—C8—H8C	109.5	H27A—C27—H27B	107.4
H8A—C8—H8C	109.5	N2—C28—C29^{i}	111.9 (3)
H8B—C8—H8C	109.5	N2—C28—H28A	109.2
O3—C9—C12	109.3 (3)	C29^{i}—C28—H28A	109.2
O3—C9—C10	110.2 (3)	N2—C28—H28B	109.2
C12—C9—C10	112.7 (4)	C29^{i}—C28—H28B	109.2
O3—C9—C11	105.6 (3)	H28A—C28—H28B	107.9
C12—C9—C11	109.4 (4)	C28^{i}—C29—N2	111.1 (3)
C10—C9—C11	109.3 (3)	C28^{i}—C29—H29A	109.4
C9—C10—H10A	109.5	N2—C29—H29A	109.4
C9—C10—H10B	109.5	C28^{i}—C29—H29B	109.4
H10A—C10—H10B	109.5	N2—C29—H29B	109.4

C9—C10—H10C	109.5	H29A—C29—H29B	108
H10A—C10—H10C	109.5	S2A—Cd1—N1	99.7 (8)
H10B—C10—H10C	109.5	S2A—Cd1—N2	86.5 (12)
C9—C11—H11A	109.5	N1—Cd1—N2	88.42 (11)
C9—C11—H11B	109.5	S2A—Cd1—S1	148.0 (13)
H11A—C11—H11B	109.5	N1—Cd1—S1	103.01 (15)
C9—C11—H11C	109.5	N2—Cd1—S1	116.12 (19)
H11A—C11—H11C	109.5	S2A—Cd1—S2	12.7 (12)
H11B—C11—H11C	109.5	N1—Cd1—S2	107.32 (14)
C9—C12—H12A	109.5	N2—Cd1—S2	96.83 (13)
C9—C12—H12B	109.5	S1—Cd1—S2	135.39 (13)
H12A—C12—H12B	109.5	S2A—Cd1—S1A	144.5 (11)
C9—C12—H12C	109.5	N1—Cd1—S1A	98.2 (5)
H12A—C12—H12C	109.5	N2—Cd1—S1A	124.5 (7)
H12B—C12—H12C	109.5	C1—O1—Si1	138.5 (3)
O4—C13—C15	111.9 (3)	C5—O2—Si1	132.7 (3)
O4—C13—C14	106.3 (3)	C9—O3—Si1	130.5 (2)
C15—C13—C14	110.9 (4)	C13—O4—Si2	132.4 (2)
O4—C13—C16	108.3 (3)	C17—O5—Si2	133.1 (2)
C15—C13—C16	110.5 (5)	C21—O6—Si2	132.6 (3)
C14—C13—C16	108.8 (4)	C25—N1—Cd1	115.1 (3)
C13—C14—H14A	109.5	C25—N1—H1A	112 (3)
C13—C14—H14B	109.5	Cd1—N1—H1A	117 (3)
H14A—C14—H14B	109.5	C25—N1—H1B	112 (3)
C13—C14—H14C	109.5	Cd1—N1—H1B	96 (3)
H14A—C14—H14C	109.5	H1A—N1—H1B	103 (4)
H14B—C14—H14C	109.5	C28—N2—C26	110.3 (3)
C13—C15—H15A	109.5	C28—N2—C29	106.9 (3)
C13—C15—H15B	109.5	C26—N2—C29	105.6 (3)
H15A—C15—H15B	109.5	C28—N2—Cd1	114.5 (3)
C13—C15—H15C	109.5	C26—N2—Cd1	107.7 (2)
H15A—C15—H15C	109.5	C29—N2—Cd1	111.5 (2)
H15B—C15—H15C	109.5	Si1—S1—Cd1	103.74 (19)
C13—C16—H16A	109.5	Si1—S1A—Cd1	95.6 (9)
C13—C16—H16B	109.5	S2A—S2—Si2	89.7 (13)
H16A—C16—H16B	109.5	S2A—S2—Cd1	67.0 (14)
C13—C16—H16C	109.5	Si2—S2—Cd1	103.75 (19)
H16A—C16—H16C	109.5	S2—S2A—Si2	75 (2)
H16B—C16—H16C	109.5	S2—S2A—Cd1	100 (2)
O5—C17—C19	109.3 (4)	Si2—S2A—Cd1	107.0 (5)
O5—C17—C20	104.7 (4)	O1—Si1—O3	111.48 (14)
C19—C17—C20	111.1 (4)	O1—Si1—O2	106.02 (15)
O5—C17—C18	109.7 (3)	O3—Si1—O2	104.32 (14)
C19—C17—C18	111.5 (4)	O1—Si1—S1	116.5 (2)
C20—C17—C18	110.3 (4)	O3—Si1—S1	107.29 (16)
C17—C18—H18A	109.5	O2—Si1—S1	110.54 (19)
C17—C18—H18B	109.5	O1—Si1—S1A	106.2 (9)
H18A—C18—H18B	109.5	O3—Si1—S1A	110.7 (5)

C17—C18—H18C	109.5	O2—Si1—S1A	118.1 (7)
H18A—C18—H18C	109.5	O6—Si2—O5	104.93 (14)
H18B—C18—H18C	109.5	O6—Si2—O4	103.50 (14)
C17—C19—H19A	109.5	O5—Si2—O4	113.26 (14)
C17—C19—H19B	109.5	O6—Si2—S2	116.43 (18)
H19A—C19—H19B	109.5	O5—Si2—S2	109.5 (2)
C17—C19—H19C	109.5	O4—Si2—S2	109.24 (12)
H19A—C19—H19C	109.5	O6—Si2—S2A	102.9 (13)
H19B—C19—H19C	109.5	O5—Si2—S2A	121.3 (10)
C17—C20—H20A	109.5	O4—Si2—S2A	108.8 (3)
C17—C20—H20B	109.5	S2—Si2—S2A	14.9 (12)

N1—C25—C27—C26	−75.9 (5)	C28^{i}—C29—N2—C26	−175.1 (3)
N2—C26—C27—C25	79.8 (5)	C28^{i}—C29—N2—Cd1	68.2 (3)
C2—C1—O1—Si1	−42.7 (7)	Cd1—S2—S2A—Si2	105.1 (5)
C3—C1—O1—Si1	79.7 (6)	Si2—S2—S2A—Cd1	−105.1 (5)
C4—C1—O1—Si1	−163.6 (5)	C1—O1—Si1—O3	99.8 (5)
C8—C5—O2—Si1	169.5 (3)	C1—O1—Si1—O2	−147.3 (5)
C7—C5—O2—Si1	49.2 (6)	C1—O1—Si1—S1	−23.8 (5)
C6—C5—O2—Si1	−71.5 (5)	C1—O1—Si1—S1A	−20.8 (7)
C12—C9—O3—Si1	−85.6 (4)	C9—O3—Si1—O1	39.4 (3)
C10—C9—O3—Si1	38.8 (5)	C9—O3—Si1—O2	−74.6 (3)
C11—C9—O3—Si1	156.7 (3)	C9—O3—Si1—S1	168.1 (3)
C15—C13—O4—Si2	−37.4 (5)	C9—O3—Si1—S1A	157.3 (10)
C14—C13—O4—Si2	−158.6 (3)	C5—O2—Si1—O1	43.1 (4)
C16—C13—O4—Si2	84.6 (5)	C5—O2—Si1—O3	160.9 (3)
C19—C17—O5—Si2	81.9 (5)	C5—O2—Si1—S1	−84.0 (4)
C20—C17—O5—Si2	−159.0 (3)	C5—O2—Si1—S1A	−75.7 (9)
C18—C17—O5—Si2	−40.7 (5)	C21—O6—Si2—O5	51.6 (3)
C22—C21—O6—Si2	−86.2 (4)	C21—O6—Si2—O4	170.6 (3)
C24—C21—O6—Si2	37.6 (6)	C21—O6—Si2—S2	−69.6 (4)
C23—C21—O6—Si2	156.4 (3)	C21—O6—Si2—S2A	−76.2 (6)
C27—C25—N1—Cd1	61.1 (4)	C17—O5—Si2—O6	−163.3 (3)
C29^{i}—C28—N2—C26	172.5 (3)	C17—O5—Si2—O4	84.6 (4)
C29^{i}—C28—N2—C29	58.2 (5)	C17—O5—Si2—S2	−37.6 (4)
C29^{i}—C28—N2—Cd1	−65.9 (4)	C17—O5—Si2—S2A	−47.6 (13)
C27—C26—N2—C28	64.6 (5)	C13—O4—Si2—O6	−58.9 (3)
C27—C26—N2—C29	179.8 (3)	C13—O4—Si2—O5	54.1 (3)
C27—C26—N2—Cd1	−61.0 (4)	C13—O4—Si2—S2	176.4 (3)
C28^{i}—C29—N2—C28	−57.7 (4)	C13—O4—Si2—S2A	−167.9 (15)

Symmetry code: (i) −*x*+2, −*y*+1, −*z*+1.

Hydrogen-bond geometry (Å, º)

D—H···*A*	*D*—H	H···*A*	*D*···*A*	*D*—H···*A*
N1—H1*A*···S1^{ii}	0.86 (5)	2.70 (5)	3.519 (5)	159 (4)

N1—H1*B*···O4	0.84 (5)	2.41 (5)	3.115 (4)	142 (4)

Symmetry code: (ii) −*x*+1, −*y*+1, −*z*+1.